Using molecular simulations for screening of zeolites for separation of CO_2/CH_4 mixtures

R. Krishna*, J.M. van Baten

Van't Hoff Institute for Molecular Sciences, University of Amsterdam, Nieuwe Achtergracht 166, 1018 WV Amsterdam, The Netherlands

Abstract

Using Grand Canonical Monte Carlo (GCMC) and molecular dynamics (MD) simulation techniques 12 different zeolites were screened to determine which one would yield the best membrane separation selectivity for separation of CO_2 and CH_4. The choice of the zeolite has a significant influence on both the sorption and diffusion selectivities. It was found that zeolites CHA and DDR, that have cages separated by narrow windows, yielded the best permeation selectivities.
© 2007 Elsevier B.V. All rights reserved.

Keywords: Zeolites; Monte Carlo; Molecular dynamics; CO_2 separation; Membrane permeation; Separation selectivity

1. Introduction

The separation of CO_2 from natural gas is an important problem. The natural gas stream is available at high pressures of a few megapascals, and can be considered to be primarily methane (CH_4). CO_2 is a longer, slender molecule; CH_4 is a more compact molecule with a slightly larger cross-section. Fig. 1 presents cartoons showing approximate molecular dimensions of CO_2, CH_4 and N_2; these dimensions were estimated using published force fields for molecule–molecule interactions [1–3]. The subtle differences in the molecular dimensions of the two molecules can be exploited by allowing them to adsorb, and subsequently diffuse, across zeolite membranes [4–6]. From a practical point of view it is advantageous to use a membrane separation process in which CH_4 is retained on the high pressure side and CO_2 permeates selectively across to the membrane. Let us define the permeation selectivity

$$\alpha_{\mathrm{perm}} = \frac{N_1/N_2}{f_1/f_2} \tag{1}$$

In Eq. (1) N_1 and N_2 represent the steady-state fluxes of $CO_2(1)$ and $CH_4(2)$ crossing the membrane and f_1 and f_2 are the partial gas phase fugacities of the two species in the upstream compartment of the membrane. The flux of any species is related to its

chemical potential gradient by the Maxwell–Stefan equations [7]

$$-\rho \frac{q_i}{RT} \nabla \mu_i = \sum_{\substack{j=1 \\ j \neq i}}^{n} \frac{q_j N_i - q_i N_j}{q_{j,\mathrm{sat}} Đ_{ij}} + \frac{N_i}{Đ_i}, \quad i = 1, \ldots, n \tag{2}$$

In Eq. (2) $Đ_i$ is the Maxwell–Stefan diffusivity of species i, q_i the molar loading, $q_{i,\mathrm{sat}}$ the saturation capacity of species i, and $Đ_{ij}$ are the binary exchange coefficients. The gradient of the chemical potentials can be related to the gradients in the loadings by defining a matrix of thermodynamic factors

$$\frac{q_i}{RT} \nabla \mu_i = \sum_{j=1}^{n} \Gamma_{ij} \nabla q_j, \quad \Gamma_{ij} \equiv \frac{q_i}{f_i} \frac{\partial f_i}{\partial q_j}, \quad i, j = 1, \ldots, n \tag{3}$$

The accurate determination of the saturation capacities $q_{i,\mathrm{sat}}$ is essential in order to estimate the diffusion fluxes in the mixture; these can be obtained from the pure component sorption isotherms provided these are available up to saturation limits.

For *screening* purposes we consider an equimolar gas mixture in the upstream compartment, i.e. $f_1 = f_2$, take the downstream loadings to be vanishingly small, and approximate Eq. (4) by

$$\alpha_{\mathrm{perm}} = \frac{D_{1,\mathrm{self}}}{D_{2,\mathrm{self}}} \frac{q_1}{q_2} = \alpha_{\mathrm{diff}} \alpha_{\mathrm{sorp}} \tag{4}$$

---

* Corresponding author. Tel.: +31 20 5257007; fax: +31 20 5255604.
E-mail address: r.krishna@uva.nl (R. Krishna).

Nomenclature

$Đ_i$	Maxwell–Stefan diffusivity of species i (m² s⁻¹)
f_i	fugacity of species i (Pa)
$\langle n_i \rangle$	ensemble average number of molecules in sampling volume
N_i	molar flux of species i across membrane (mol m⁻² s⁻¹)
q_i	molar loading (mol/kg)
$q_{i,\text{sat}}$	saturation loading (mol/kg)
R	gas constant (8.314 J mol⁻¹ K⁻¹)
T	absolute temperature (K)

Greek letters

α_{diff}	diffusion selectivity
α_{perm}	permeation selectivity
α_{sorp}	sorption selectivity
Γ_{ij}	thermodynamic factors
θ_i	fractional occupancy of component i
μ_i	molar chemical potential (J mol⁻¹)
ρ	density of zeolite (kg m⁻³)

Subscript

sat	referring to saturation conditions

where the diffusion selectivity α_{diff} is the ratio of the self-diffusivities of components 1 and 2, i.e.

$$\alpha_{\text{diff}} = \frac{D_{1,\text{self}}}{D_{2,\text{self}}} \tag{5}$$
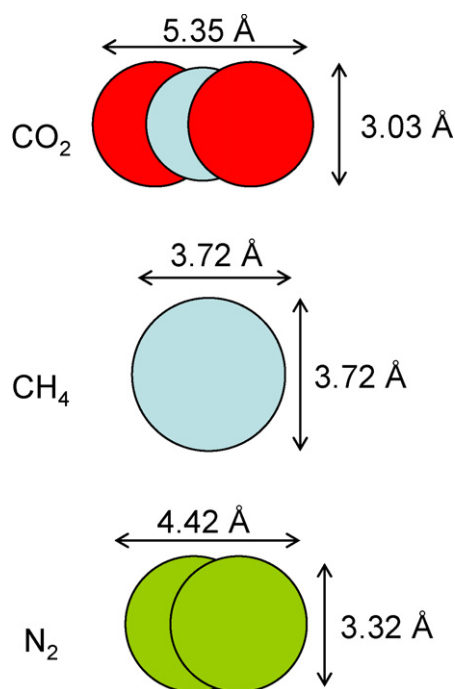

Fig. 1. Cartoon showing the approximate molecular dimensions of CO_2, CH_4 and N_2.

and the sorption selectivity α_{sorp} is defined as the ratio of the molar loadings q_i of CO_2 and CH_4 at the upstream face of the membrane

$$\alpha_{\text{sorp}} = \frac{q_1}{q_2} \tag{6}$$

Recent development in Monte Carlo (MC) and molecular dynamics (MD) simulation techniques, coupled with the availability of high performance computing facilities, have enabled the determination of the adsorption and diffusion characteristics of a variety of molecules in different zeolites with a reasonable degree of accuracy and reliability [8–12]. An earlier study showed the utility of molecular simulations in screening zeolites for separation of hexane isomers [13]. The major objective of the current study is to illustrate the potential of MC and MD simulations in screening zeolites for separation of CH_4 and CO_2 for maximum permeation selectivity. We evaluate various zeolites in with regard to α_{sorp} and, subsequently, α_{diff}. We demonstrate that molecular simulations can provide insights into adsorption mechanisms, siting, orientation, and transport of molecules that are not available from experiments alone. Such insights allow the development of more fundamental models for process design.

2. Simulation results and discussion

More than 180 zeolite structures are known [14]. Fig. 2 shows some common topologies. The adsorption isotherms for pure CO_2, pure CH_4 and equimolar binary mixtures of CO_2 and CH_4 at 300 K in 12 different zeolites were computed using the Grand Canonical Monte Carlo (GCMC) technique. The chosen zeolites fall into three categories consisting of (a) one-dimensional channel structures (AFI, MOR, TON, FER, LTL), (b) intersecting channels (MFI, ISV, BEA), and (c) cages separated by windows (FAU, LTA, CHA, DDR). The simulation methodology, including a description of the force field, is given in Supplementary Data, that includes the complete set of information on the adsorption isotherms, along with snapshots showing the location of the molecules in the various zeolite structures. A selection of the important results is presented and discussed below.

Consider the pure component sorption isotherms of CO_2 and CH_4 in MFI determined experimentally by Zhu et al. [6], Golden and Sircar [15] and Kishima et al. [16]; see Fig. 3a and b. As is conventional, the data are plotted on linear axes. Zhu et al. [6] fitted the data with a single site Langmuir model with saturation capacities of 2.97 and 2.69 mol/kg for CO_2 and CH_4, respectively. When the same experimental data set is plotted with a logarithmic scale for the pressure axis it becomes apparent that for the range of pressures used in the experiments saturation was not achieved; see Fig. 3c and d. Also plotted in Fig. 3c and d are the GCMC simulation results that can be carried out to pressures say of 10^{11} Pa that are not accessible experimentally. The GCMC simulations suggest saturation capacities of 5.8 and 4 mol/kg for CO_2 and CH_4, respectively. These values correspond to values determined assuming that the pore volume is filled with saturated liquid.
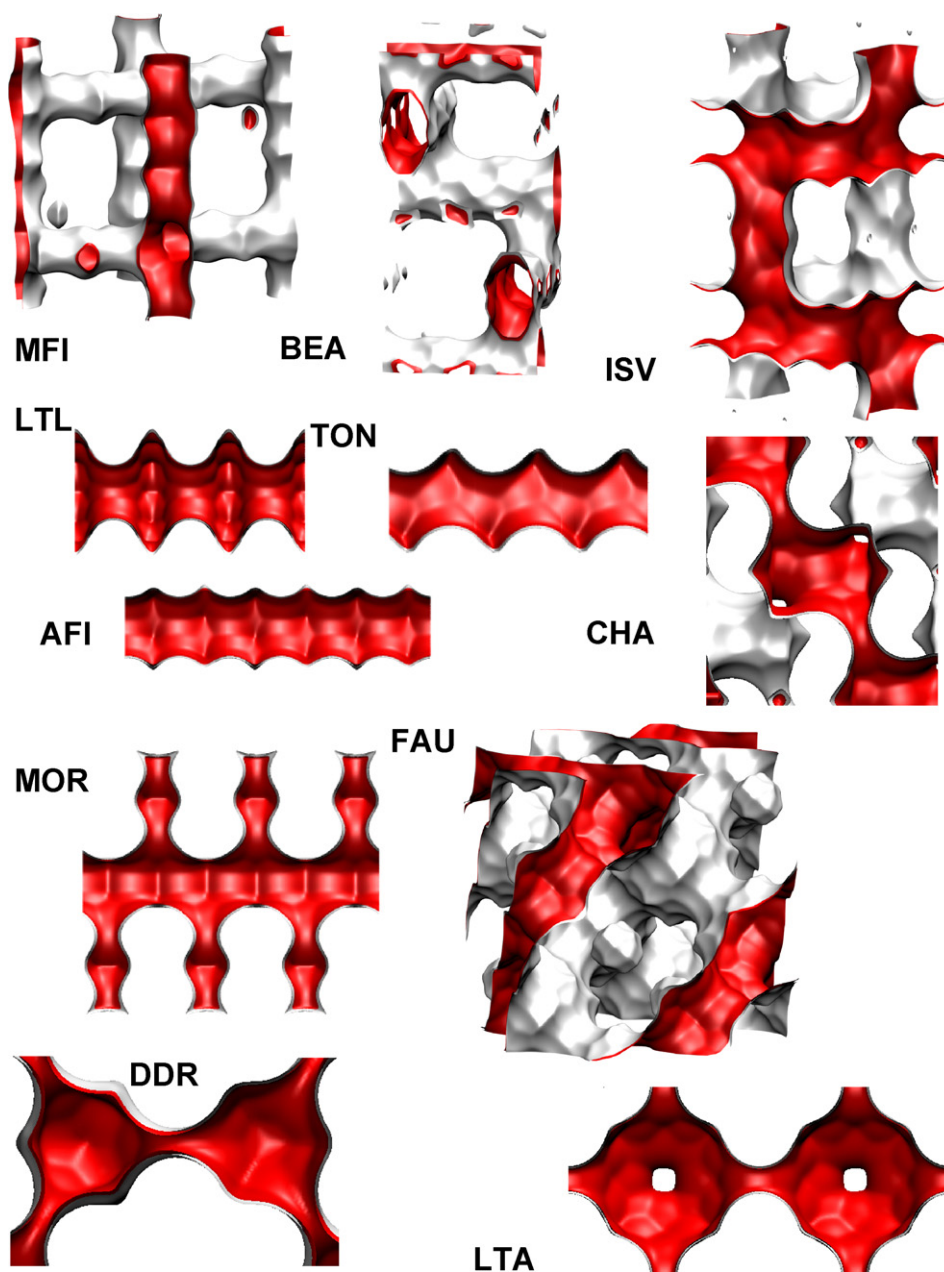
Fig. 2. A selection of zeolite structures. Note that the individual landscapes of zeolites are not all drawn to the same scale.

Fig. 4 shows the experimental data of Himeno et al. [17], indicated by the open symbols, for pure component isotherms of CO_2 and CH_4 in DDR for temperatures of (a) 273 K, (b) 298 K, (c) 323 K, and (d) 348 K. The filled symbols are GCMC simulation results; there is good agreement between the experiments and GCMC simulations confirming the correctness of the force field used in the simulations. On the basis of their experimental data Himeno et al. [17] obtained saturation capacities of approximately 2.8 and 1.7 mol/kg for CO_2 and CH_4, respectively. The GCMC simulation results appear to indicate that saturation was not achieved in the experiments and the true saturation capacities are significantly higher, about 4.6 and 4.2 mol/kg, for CO_2 and CH_4, respectively.

A further cautionary note is required when fitting of experimental isotherm data for CO_2 and CH_4. In almost all zeolites these molecules show inflection behavior and therefore a simple single site Langmuir fit is not justified. At least two-site, in most cases three-site Langmuir isotherm fits will be required [18]. This further underlines the problem of determining the saturation capacities from experimental isotherms an isotherm inflection can be mistaken to indicate saturation.
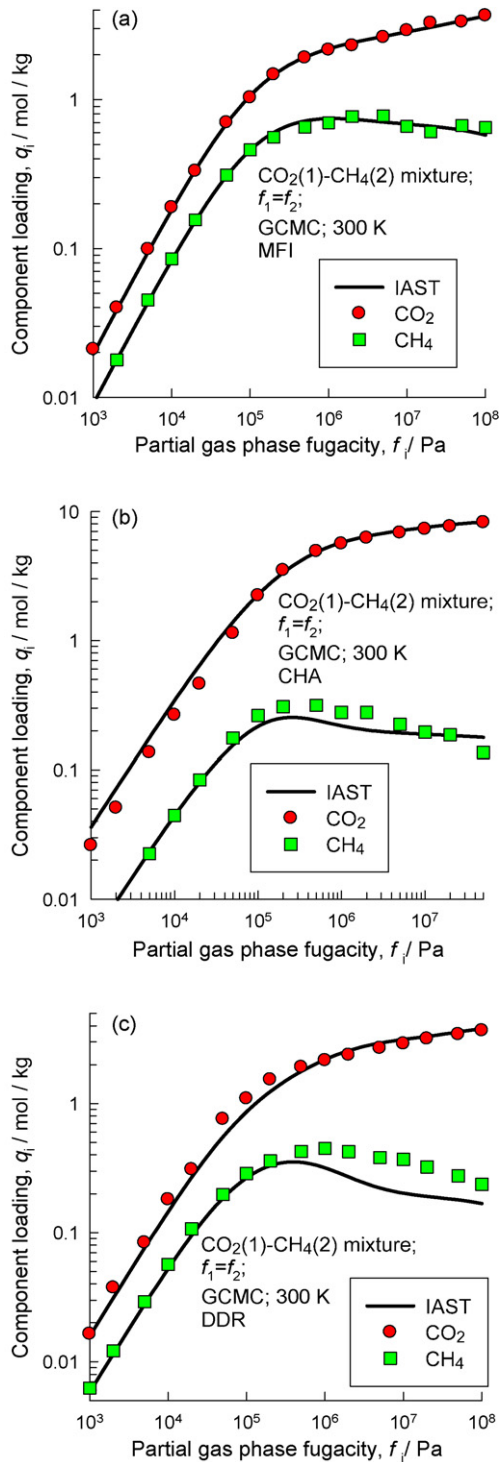
GCMC simulations for the component loadings in equilibrium with an equimolar gas mixture of CO_2 and CH_4 in (a) MFI, (b) CHA, and (c) DDR at 300 K are shown in Fig. 5. With increasing pressure the selectivity increases in favor of CO_2; the use of the multicomponent Langmuir model will yield selec-
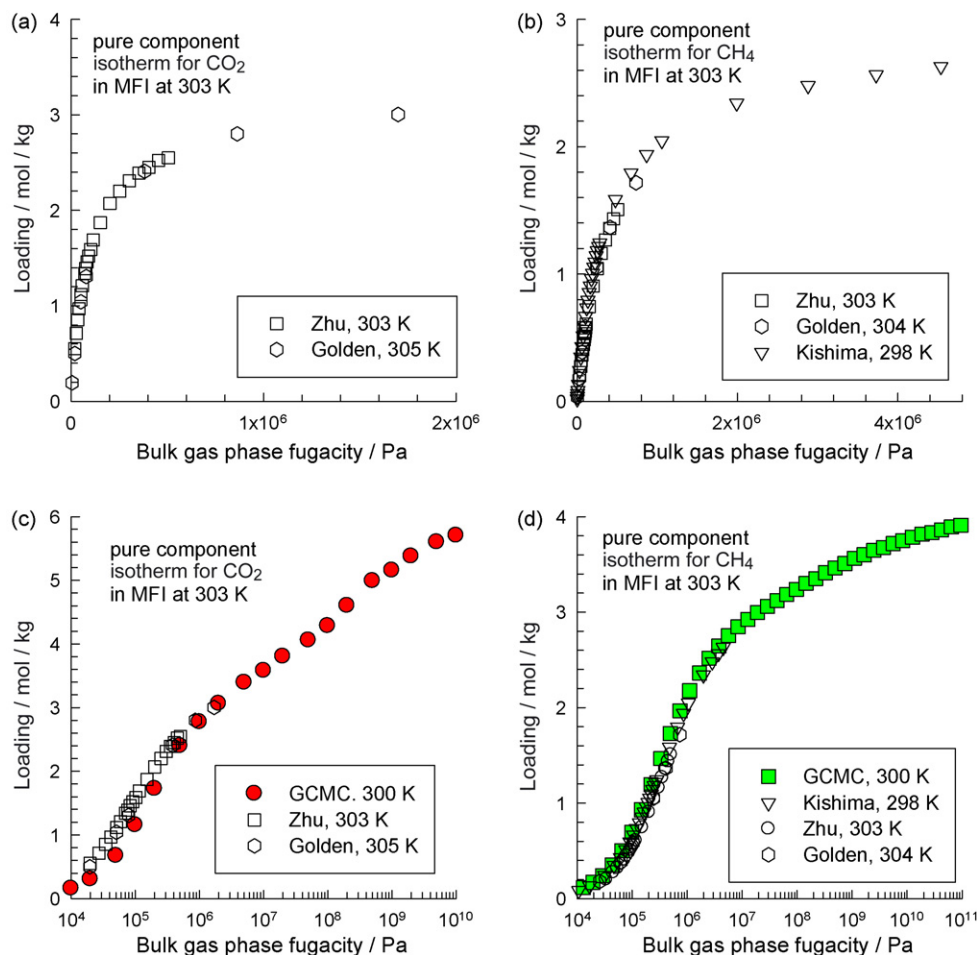
Fig. 3. Pure component sorption isotherm data for (a and c) CO_2 and (b and d) CH_4 in MFI at 298–305 K. The filled symbols are GCMC simulation results. The open symbols are experimental data of Zhu et al. [6], Golden and Sircar [15] and Kishima et al. [16].

tivities that are independent of the loadings and the pressure. Since the saturation capacities of CO_2 and CH_4 are significantly different from each other, the multicomponent Langmuir model cannot be used to calculate the component loadings for binary mixture sorption because of thermodynamic inconsistencies [19]. The continuous solid lines in Fig. 5 represent calculations of the IAST [20] using three-site Langmuir fits of pure component isotherms as given in an earlier publication [18]. The IAST provides a reasonable accurate estimation of loadings in the mixture and is recommended for use for process design.

The sorption selectivity $\alpha_{sorp} = q_1/q_2$ was determined from the component loadings for 12 different zeolites, divided into three categories: (a) uni-dimensional channels, (b) intersecting channels, and (c) cages-separated-by-windows; see Fig. 6. In all cases $\alpha_{sorp} = q_1/q_2$ increases with increasing values of $q = q_1 + q_2$. In order to verify that the separation selectivity hierarchy is not influenced by the presence of other species present in natural gas, such as N_2, simulations were also carried out for a mixture $CO_2/CH_4/N_2$; the results for $\alpha_{sorp} = q_1/q_2$ in this ternary mixture are presented in Fig. 7; the results show that the values of α_{sorp} are practically identical to the ones obtained in

the binary mixture. On the basis of the simulation data on α_{sorp} we can narrow the choice of zeolite to MOR, LTL, MFI, CHA and DDR. We consider each of these zeolites in turn. We note that the α_{sorp} value for these zeolites are significantly higher than that of MWW, as reported in a recent molecular simulation study [21].

Let us first try to rationalize the α_{sorp} values observed for MOR at *low* loadings. For this purpose we examine the pure component sorption isotherms; see Fig. 8a. At pressures below about 20 kPa there is practically no adsorption of CH_4 while there is a finite adsorption of CO_2. The GCMC simulation results are in agreement with the experimental data (open symbols) of Delgado et al. [22] for H-MOR. A snapshot of CO_2 molecules within MOR at 300 K and $p = 10$ kPa is given in Fig. 8b; this shows that the CO_2 are exclusively located within the side pockets of MOR. Location within side pockets is not very effective during membrane permeation as the molecules cannot diffuse out, except via the main 12-ring channels. In order to confirm this we carried out MD simulations to determine self-diffusivities in an equimolar mixture of CO_2 and CH_4 in MOR at 300 K. The ratio of the self-diffusivities approximates α_{diff} and this data is presented in Fig. 8c. At low loadings the diffusivity of CO_2
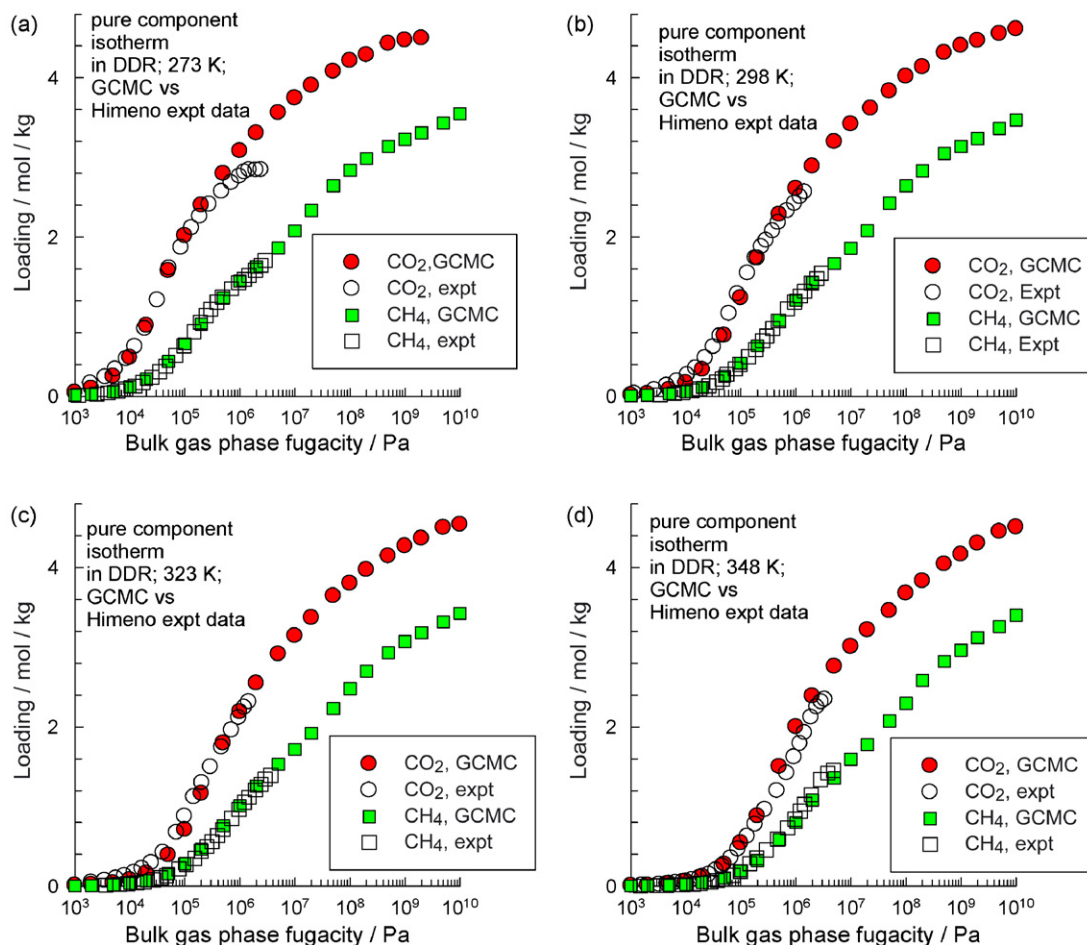
Fig. 4. Pure component sorption isotherm data for CO_2 and CH_4 in DDR at (a) 273 K, (b) 298 K, (c) 323 K, and (d) 348 K. The filled symbols are GCMC simulation results. The open symbols are experimental data of Himeno et al. [17] for DDR.

is about one order of magnitude lower than that of CH_4; this confirms the idea that at low loadings a vast majority of the CO_2 are trapped in the side pockets. Furthermore, we note that loadings in excess of 2 mol/kg the diffusivities of both species are practically the same. Molecular jumps in uni-dimensional channels are strongly correlated and both species have the same effective mobility; consequently $\alpha_{diff} \approx 1$. An analogous picture holds for transport within the uni-dimensional channels of LTL; for this zeolite too the α_{diff} reach values of unity as the loading is increased above 2 mol/kg; see Fig. 8c. Let us turn to MFI which has an intersecting channel structure; see snapshot in Fig. 9a. Within the intersecting channels of MFI the molecular jumps of CO_2 and CH_4 are also strongly correlated [3] and therefore the values of α_{diff}, have values close to unity; cf. Fig. 8c.

The situation with respect to diffusion in CHA and DDR, both having cages separated by narrow windows, is different. Here the inter-cage hops of molecules through the narrow windows separating the two cages occur practically independently of one another because only one molecule can pass through a window at a given time [3]; see snapshots in Fig. 9b and c. CO_2 is a more slender molecule than CH_4,

and the values of α_{diff} for CHA and DDR are significantly higher than unity; see Fig. 8c. The window size for DDR is smaller than that of CHA and this is the reason for its higher α_{diff}.

The differences in the mixture diffusion characteristics of various zeolite structures are also emphasized in earlier publications [23,24].

Fig. 10 summarizes the data on the permeation selectivity, α_{perm}, obtained as a product α_{sorp} and α_{diff}, as a function of total loading q for MFI, MOR, LTL, CHA and DDR zeolites. We see that the choice of ideal zeolite for use in membrane separations is between CHA and DDR. Also shown by filled symbols in Fig. 10 are experimental permeation selectivities as measured in DDR by van den Bergh et al. [25], and in SAPO-34, an isotype of CHA, by Li et al. [26,27]. The reasonably good agreement between the experimental permeation selectivities and calculations based on molecular simulations bear testimony to the accuracy and applicability of the approach followed in this paper. We also note that the permeation selectivities for CHA and DDR membranes are significantly higher than those obtained from FAU membranes with different Si/Al ratios [28].

Fig. 5. GCMC simulations for the component loadings in equilibrium with an equimolar gas mixture of CO_2 and CH_4 in (a) MFI, (b) CHA, and (c) DDR at 300 K. The continuous solid lines represent calculations of the IAST [20] using three-site Langmuir fits of pure component isotherms; these fit parameters are given in Appendix A1 of the Supplementary Data accompanying this publication.
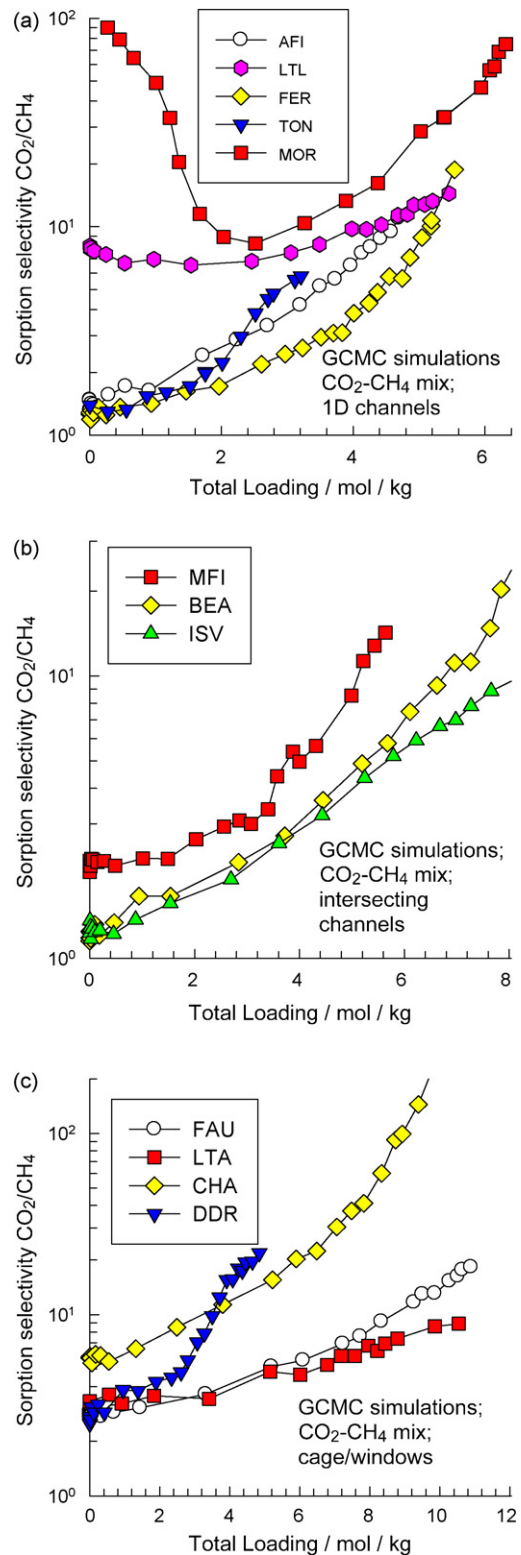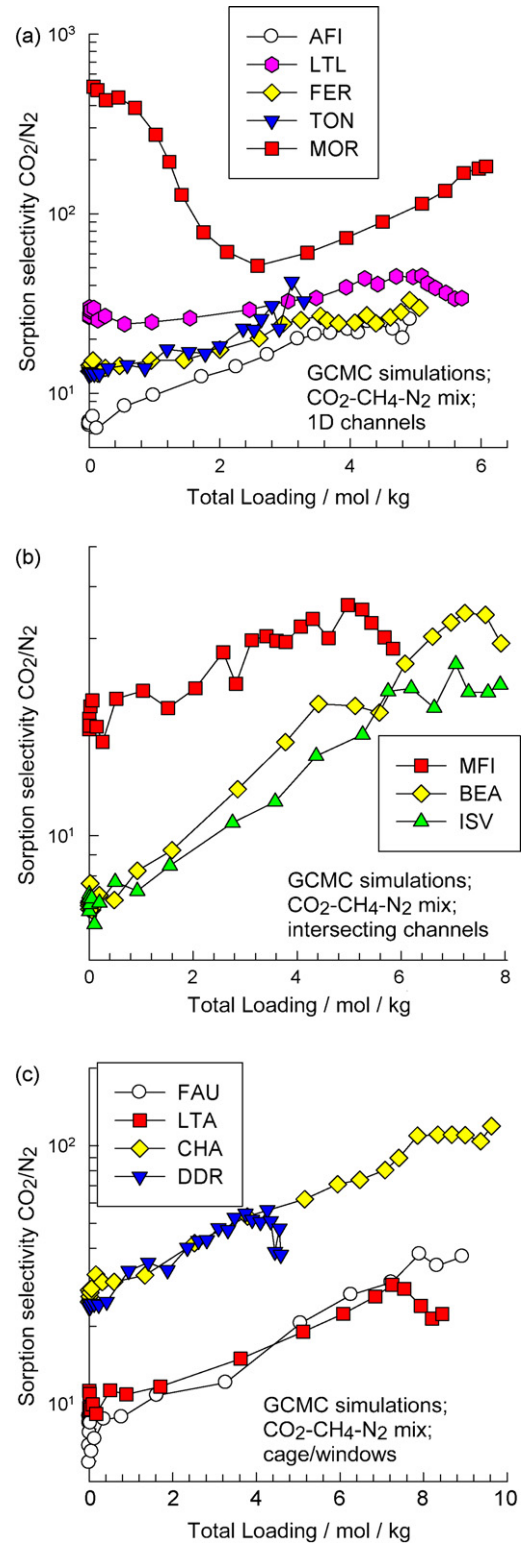

Fig. 6. CO_2/CH_4 sorption selectivity $\alpha_{sorp} = q_1/q_2$ as a function of the total mixture loading $q = q_1 + q_2$, determined from GCMC binary mixture simulations, determined from GCMC simulations taking $f_1 = f_2$, for (a) one-dimensional channel structures (AFI, MOR, TON, FER, LTL), (b) intersecting channels (MFI, ISV, BEA), and (c) cages separated by windows (FAU, LTA, CHA, DDR).
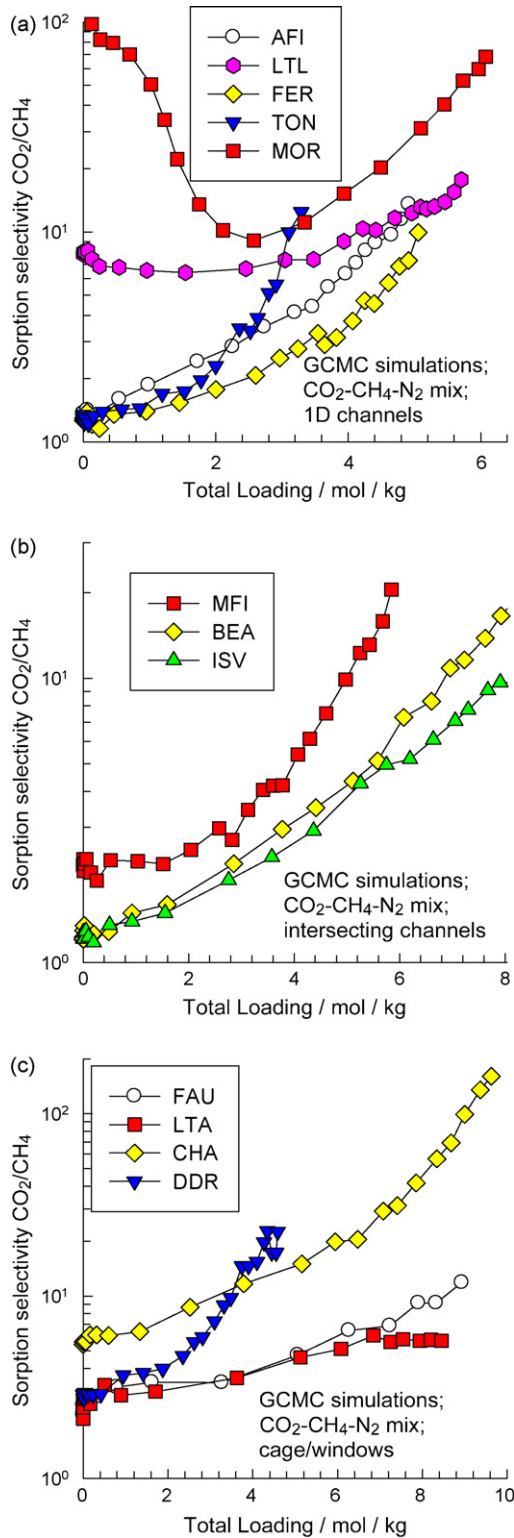
Fig. 7. CO_2/CH_4 sorption selectivity $\alpha_{sorp} = q_1/q_2$ as a function of the total mixture loading $q = q_1 + q_2 + q_3$ in ternary mixture $CO_2/CH_4/N_2$, determined from GCMC simulations taking $f_1 = f_2 = f_3$.
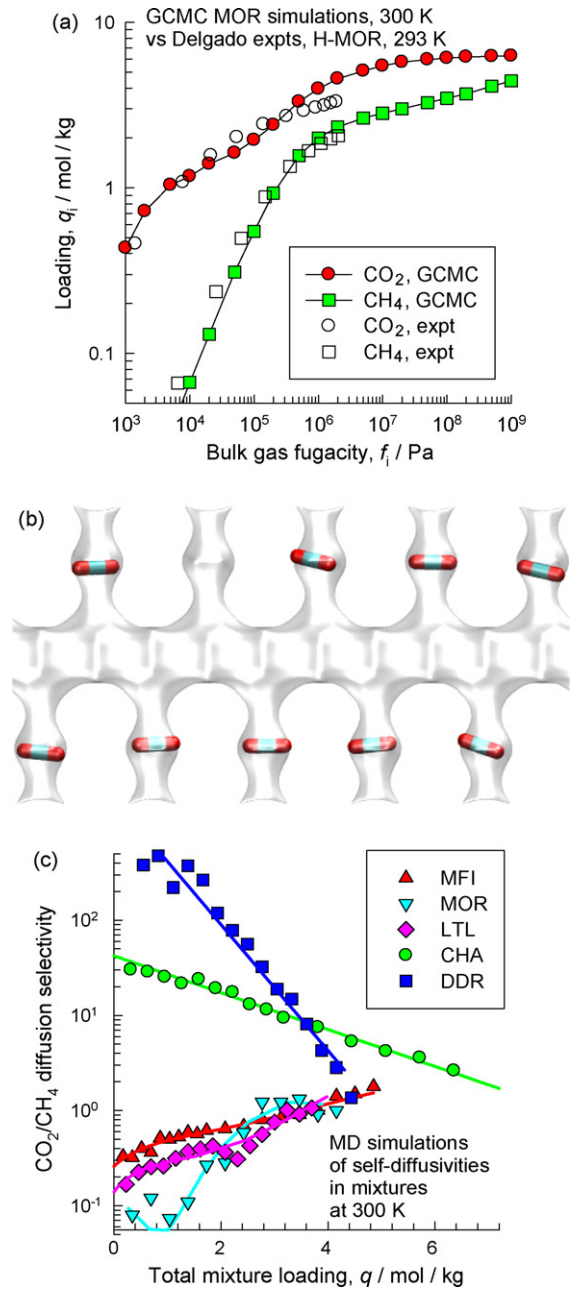
Fig. 8. (a) Pure component isotherm data for CO_2 and CH_4 in MOR at 300 K. Also shown are the experimental data (open symbols) of Delgado et al.[22] for H-MOR. (b) Snapshot of CO_2 in MOR at 300 K and $p = 10$ kPa. (c) The diffusion selectivity α_{diff} for various zeolites, calculated on the basis of MD simulations of self-diffusivities mixtures. The self-diffusivity data in for MFI, MOR and LTL are based on simulations of 1:1 mixtures of CO_2 and CH_4. For DDR and CHA the presented data are for 3:1 and 10:1 mixtures, respectively, in order to reflect the higher sorption selectivities for the zeolites.

(a)

(b)

(c)
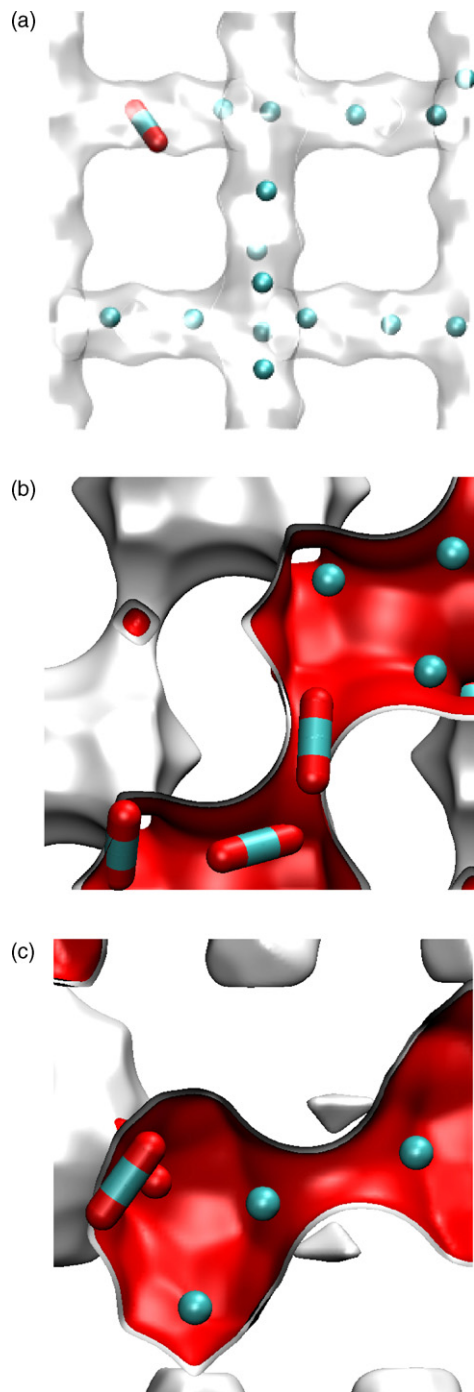
Fig. 9. Snapshots of CO_2 and CH_4 in (a) MFI, (b) CHA, and (c) DDR. These snapshots were made at partial fugacities of 500 and 9500 kPa, respectively for CO_2 and CH_4. Note that the individual snapshots are not all drawn to the same scale.

Fig. 10. The permeation selectivity, α_{perm} as a function of total loading q for MFI, MOR, LTL, CHA and DDR zeolites. Also shown by filled symbols are the experimental permeation selectivity data for DDR [25], and SAPO-34 [26,27].

The permeation selectivity calculations using α_{perm} are good enough for screening purposes. For accurate process design calculations of the fluxes using the M-S equations we need the matrix of thermodynamic factor $[\Gamma]$ in Eq. (3). The fluctuation formula of Reed and Ehrlich [29] can be extended to a binary mixture to obtain the following expression for the *inverse* matrix of thermodynamic factors $[L]$:

$$L_{ji} \equiv \frac{f_i}{q_i}\frac{\partial q_j}{\partial f_i} = \frac{\langle n_i n_j \rangle - \langle n_i \rangle \langle n_j \rangle}{\langle n_i \rangle} \tag{7}$$

The desired elements of the matrix of thermodynamic factors $[\Gamma]$ are obtained by matrix inversion:

$$[\Gamma] = [L]^{-1} \tag{8}$$

GCMC simulations using Eq. (8) of $[\Gamma]$ for CO_2 (1)–CH_4 (2) mixtures in MFI, CHA, and DDR at 300 K are shown in Fig. 11. The continuous solid lines represent calculations of $[\Gamma]$ with IAST [20] using three-site Langmuir fits of pure component isotherms. It can be concluded that the IAST is of reasonable accuracy in process design calculations of the membrane permeation fluxes.

The procedure outlined above for screening of zeolites for CO_2/CH_4, separation can also be applied for separation of CO_2/N_2. Fig. 12 shows the CO_2/N_2 sorption selectivity, $\alpha_{sorp} = q_1/q_3$, as a function of the total mixture loading $q = q_1 + q_2 + q_3$ in ternary mixture $CO_2/CH_4/N_2$, determined from GCMC simulations taking $f_1 = f_2 = f_3$. We conclude from this figure that the highest sorption selectivities are obtained with CHA zeolite. MD simulation results for self diffusivities in CO_2/N_2 mixtures in CHA are shown in Fig. 13a. We note that the diffusivity of CO_2 is smaller than that of N_2. Fig. 13b shows that the calculations of the α_{perm} for CHA compare reasonably well with the experimental data for Li et al. [26,27] for SAPO-34 membrane; the permeation selectivity values are in the range of 30–35, significantly higher than the values reported by Bernal et al. [30] for MFI membrane. We also note that our study contradicts the conclusions of Jia and Murad [31] who used MD simulations to conclude that the separation selectivity of CHA is lower than that of MFI and FAU.
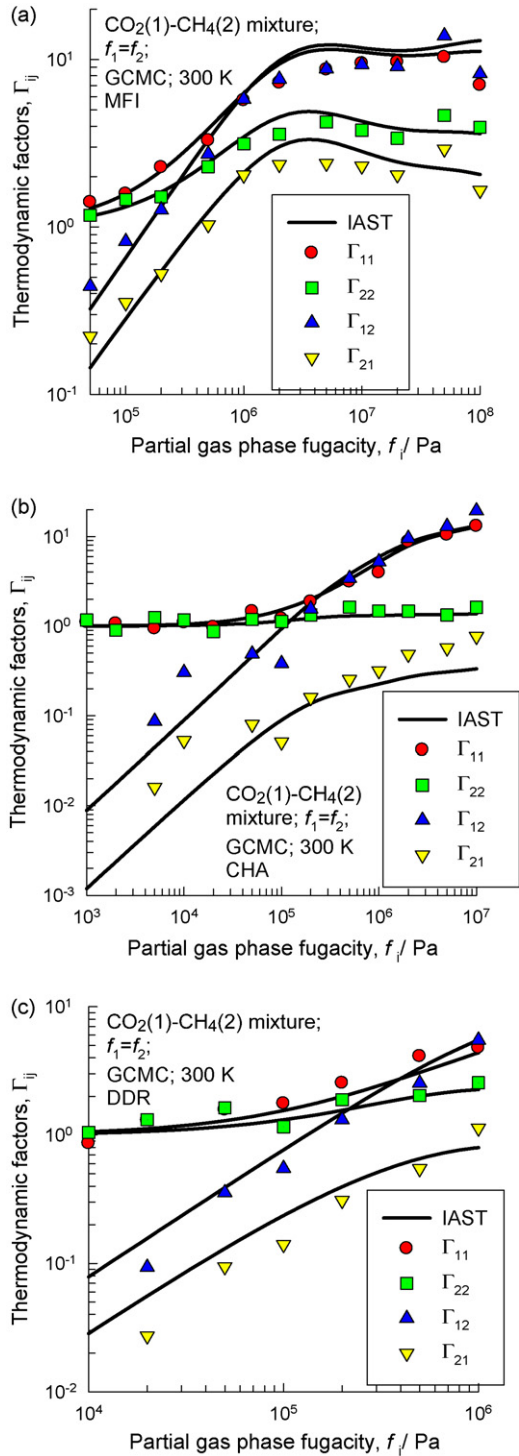
Fig. 11. GCMC simulations using Eq. (8) of $[\Gamma]$ for $CO_2(1)$–$CH_4(2)$ mixtures in (a) MFI, (b) CHA, and (c) DDR at 300 K. The continuous solid lines represent calculations of $[\Gamma]$ with IAST [20] using three-site Langmuir fits of pure component isotherms; these fit parameters are given in Appendix A1 of the Supplementary Data accompanying this publication.

Fig. 12. CO_2/N_2 sorption selectivity $\alpha_{sorp} = q_1/q_3$ as a function of the total mixture loading $q = q_1 + q_2 + q_3$ in ternary mixture $CO_2/CH_4/N_2$, determined from GCMC simulations taking $f_1 = f_2 = f_3$.
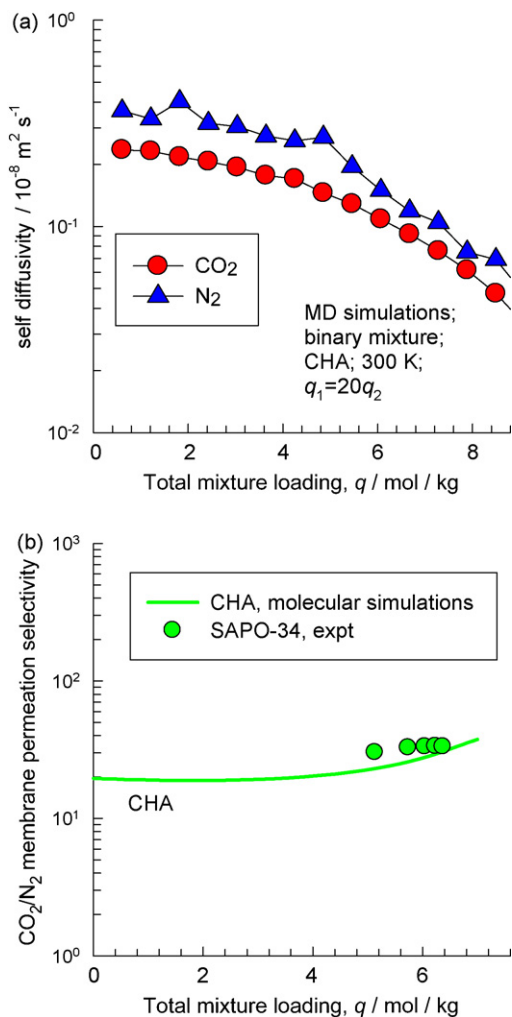
Fig. 13. (a) The CO_2/N_2 diffusion selectivity α_{diff} for CHA, calculated on the basis of MD simulations of self-diffusivities mixtures. The presented data are for 20:1 mixtures in order to reflect the higher sorption selectivities for the zeolites. (b) The CO_2/N_2 permeation selectivity, α_{perm} as a function of total loading q for CHA zeolite. Also shown by filled symbols are the experimental permeation selectivity data for SAPO-34 [26,27].

3. Conclusions

Twelve different zeolites were screened using GCMC and MD simulation to determine which one would lead to the best permeation selectivity α_{perm} in a membrane process for separation of CO_2 and CH_4. On the basis of sorption selectivities α_{sorp} the choice is narrowed to MOR, LTL, MFI, CHA and DDR. In one-dimensional channel structures (MOR, LTL) and in intersecting channel structures (MFI) there is strong correlation between the molecular jumps and therefore the diffusion selectivity α_{diff} is close to unity. High values of α_{diff} is achieved by choosing structures in which molecular jumps are uncorrelated; this is the case for zeolites, such as CHA and DDR, that consist of cages separated by narrow windows. CO_2 being a longer and slender molecule has a significantly higher diffusivity in such structures. Our study shows that highest α_{perm} is obtained using CHA and DDR. From a practical point of view other factors such as membrane permeation fluxes would also

need to be considered in the final choice of zeolite membrane. Other considerations that impact on the choice of the zeolite membrane used include Si/Al ratio, membrane thickness, and characteristics of support layer.

Though the emphasis in this paper has been on screening of zeolites, molecular simulation data can also be used for process design and with continued advancement it may be reasonable to expect that processes can be developed and designed entirely *in silico*.

Acknowledgements

Appendix A. Supplementary data

Supplementary data associated with this article can be found, in the online version, at doi:10.1016/j.cej.2007.02.011.

References

[1] D. Dubbeldam, S. Calero, T.J.H. Vlugt, R. Krishna, T.L.M. Maesen, B. Smit, United atom forcefield for alkanes in nanoporous materials, J. Phys. Chem. B 108 (2004) 12301–12313.

[2] K. Makrodimitris, G.K. Papadopoulos, D.N. Theodorou, Prediction of permeation properties of CO_2 and N_2 through silicalite via molecular simulations, J. Phys. Chem. B 105 (2001) 777–788.

[3] R. Krishna, J.M. van Baten, E. García-Pérez, S. Calero, Diffusion of CH_4 and CO_2 in MFI, CHA and DDR zeolites, Chem. Phys. Lett. 429 (2006) 219–224.

[4] T. Tomita, K. Nakayama, H. Sakai, Gas separation characteristics of DDR type zeolite membrane, Micropor. Mesopor. Mater. 68 (2004) 71–75.

[5] S. Li, J.G. Martinek, J.L. Falconer, R.D. Noble, T.Q. Gardner, High-pressure CO_2/CH_4 separation using SAPO-34 membranes, Ind. Eng. Chem. Res. 44 (2005) 3220–3228.

[6] W. Zhu, P. Hrabanek, L. Gora, F. Kapteijn, J.A. Moulijn, Role of adsorption in the permeation of CH_4 and CO_2 through a silicalite-1 membrane, Ind. Eng. Chem. Res. 45 (2006) 767–776.

[7] R. Krishna, J.M. van Baten, Describing binary mixture diffusion in carbon nanotubes with the Maxwell–Stefan equations. An investigation using molecular dynamics simulations, Ind. Eng. Chem. Res. 45 (2006) 2084–2093.

[8] J. Kärger, S. Vasenkov, S.M. Auerbach, Diffusion in zeolites, in: S.M. Auerbach, K.A. Carrado, P.K. Dutta (Eds.), Handbook of Zeolite Science and Technology, Marcel Dekker, New York, 2003, pp. 341–422 (Chapter 10).

[9] D. Frenkel, B. Smit, Understanding Molecular Simulations: From Algorithms to Applications, 2nd ed., Academic Press, San Diego, 2002.

[10] A.H. Fuchs, A.K. Cheetham, Adsorption of guest molecules in zeolitic materials: computational aspects, J. Phys. Chem. B 105 (2001) 7375–7383.

[11] B. Smit, R. Krishna, Molecular simulations in zeolitic process design, Chem. Eng. Sci. 58 (2003) 557–568.

[12] R. Krishna, B. Smit, S. Calero, Entropy effects during sorption of alkanes in zeolites, Chem. Soc. Rev. 31 (2002) 185–194.

[13] R. Krishna, J.M. van Baten, Screening of zeolite adsorbents for separation of hexane isomers: a molecular simulation study, Sep. Purif. Technol. 55 (2007) 246–255, doi:10.1016/j.seppur.2006.12.01.

[14] C. Baerlocher, W.M. Meier, D.H. Olson, Atlas of Zeolite Framework Types, 5th ed., Elsevier, Amsterdam, 2002.

[15] T.C. Golden, S. Sircar, Gas-adsorption on silicalite, J. Coll. Interf. Sci. 162 (1994) 182–188.

[16] M. Kishima, H. Mizuhata, T. Okubo, Effects of confinement on the adsorption behavior of methane in high-silica zeolites, J. Phys. Chem. B 110 (2006) 13889–13896.

[17] S. Himeno, T. Tomita, K. Suzuki, S. Yoshida, Characterization and selectivity for methane and carbon dioxide adsorption on the all-silica DD3R zeolite, Micropor. Mesopor. Mater. 98 (2007) 62–69.

[18] R. Krishna, J.M. van Baten, E. García-Pérez, S. Calero, Incorporating the loading dependence of the Maxwell–Stefan diffusivity in the modeling of CH_4 and CO_2 permeation across zeolite membranes, Ind. Eng. Chem. Res. 46 (2007), doi:10.1021/ie060693d.

[19] M.B. Rao, S. Sircar, Thermodynamic consistency for binary gas adsorption equilibria, Langmuir 15 (1999) 7258–7267.

[20] A.L. Myers, J.M. Prausnitz, Thermodynamics of mixed gas adsorption, AIChE J. 11 (1965) 121–130.

[21] J.M. Leyssale, G.K. Papadopoulos, D.N. Theodorou, Sorption thermodynamics of CO_2, CH_4, and their mixtures in the ITQ-1 zeolite as revealed by molecular simulations, J. Phys. Chem. B 110 (2006) 22742–22753.

[22] J.A. Delgado, M.A. Uguina, J.M. Gómez, L. Ortega, Adsorption equilibrium of carbon dioxide, methane and nitrogen onto Na- and H-mordenite at high pressures, Sep. Purif. Technol. 48 (2006) 223–228.

[23] R. Krishna, J.M. van Baten, A molecular dynamics investigation of diffusion of methane–ethane and methane–propane mixtures in zeolites, Chem. Eng. Technol. 29 (2006) 1429–1437.

[24] R. Krishna, J.M. van Baten, Diffusion of alkane mixtures in MFI zeolite, Micropor. Mesopor. Mater. (2007), doi:10.1016/j.micromeso.2006.11.032.

[25] J. van den Bergh, W. Zhu, J.C. Groen, F. Kapteijn, J.A. Moulijn, K. Yajima, K. Nakayama, T. Tomita, S. Yoshida, Natural gas purification with a ddr zeolite membrane; permeation modelling with Maxwell–Stefan equations, in: Proceedings of the 15th International Zeolite Conference, Beijing, China, 2007.

[26] S. Li, J.L. Falconer, R.D. Noble, R. Krishna, Modelling permeation of CO_2/CH_4, CO_2/N_2, and N_2/CH_4 mixtures across SAPO-34 membrane with the Maxwell–Stefan equations, Ind. Eng. Chem. Res. 46 (2007), doi:10.1021/ie0610703.

[27] S. Li, J.L. Falconer, R.D. Noble, R. Krishna, Interpreting unary, binary and ternary mixture permeation across a SAPO-34 membrane with loading-dependent Maxwell–Stefan diffusivities, J. Phys. Chem. C 111 (2007), doi:10.1021/jp067404j.

[28] Y. Hasegawa, T. Tanaka, K. Watanabe, B.H. Jeong, K. Kusakabe, S. Morooka, Separation of CO_2–CH_4 and CO_2–N_2 systems using ion-exchanged FAU-type zeolite membranes with different Si/Al ratios, Kor. J. Chem. Eng. 19 (2002) 309–313.

[29] D.A. Reed, G. Ehrlich, Surface diffusion, atomic jump rates and thermodynamics, Surf. Sci. 102 (1981) 588–609.

[30] M.P. Bernal, J. Coronas, M. Menendez, J. Santamaria, Separation of CO_2/N_2 mixtures using MFI-type zeolite membranes, AIChE J. 50 (2004) 127–135.

[31] W. Jia, S. Murad, Separation of gas mixtures using a range of zeolite membranes: a molecular-dynamics study, J. Chem. Phys. 122 (2005) 234708.

Supplementary data to accompany:

Using molecular simulations for screening of zeolites for separation of CO_2/CH_4 mixtures

R. Krishna*, J.M. van Baten

Van 't Hoff Institute for Molecular Sciences, University of Amsterdam, Nieuwe Achtergracht 166,

1018 WV Amsterdam, The Netherlands.

Contents:

Appendix A1 includes a short description of the force field and methodology used in the GCMC and MD simulations for isotherms and diffusivities of CO_2 and CH_4, including validation of force field.

Appendix A2 contains complete data on the GCMC simulation results for sorption of pure CH_4, CO_2, N_2, and equimolar CH_4/CO_2 and $CH_4/CO_2/N_2$ mixtures in different zeolite topologies; this also includes snapshots of the location of the molecules in various frameworks. Also presented in Appendix A2 are the MD simulation results for pure components and CO_2/CH_4 and CO_2/N_2 mixtures.

Appendix A1: Simulation methodologies

1. GCMC simulation methodology

The adsorption isotherms for CO_2, CH_4, and N_2, both for pure components and binary and ternary mixtures, in twelve different all-silica zeolites were computed using Monte Carlo (MC) simulations in the grand canonical (GC) ensemble. The crystallographic data are available elsewhere[1]. The zeolite lattices are rigid during simulations, with static atomic charges that are assigned by choosing $q_{Si} = +2.05$ and $q_O = -1.025$, following the work of Calero et al.[2] CH_4 molecules are described with a united atom model, in which each molecule is treated as a single interaction center[3]. CO_2 molecules are taken linear and rigid, with bond length C-O of 1.16Å and partial charges distributed around each molecule to reproduce experimental quadrupole moment. The interaction between adsorbed molecules is described with Coulombic and Lennard-Jones terms. The parameters for CH_4 are taken from Dubbeldam et al.[4] For CO_2 and N_2 we use the 3LJ3CB.EPM2 and 2LJ3CB.MSKM potentials[5]. The Lennard-Jones parameters for CH_4-zeolite, CO_2-zeolite and N_2-zeolite interactions are taken from Dubbeldam et al.[4] and Makrodimitris et al.[6]. Table 1 presents a summary of the force fields used in this study. Detailed validation of the force fields used for CH_4, CO_2 and N_2 are available elsewhere[4, 7].

The Lennard-Jones potentials are shifted and cut at 12 Å. The number of unit cells in the simulation box was chosen such that the minimum length in each of the coordinate directions was larger than 24 Å. Periodic boundary conditions were employed. Further GCMC simulation details are available in earlier publications. [2, 4, 8]

The GCMC simulations were performed using the BIGMAC code developed by T.J.H. Vlugt[9] as basis. The code was modified to handle rigid molecular structures and charges. S. Calero is gratefully acknowledged for her technical inputs in this regard.

Table 2 gives a summary of the 3-site Langmuir parameters for CO_2 and CH_4 in MFI, CHA and DDR. These parameter fits were used, along with IAST, to calculate Also presented in Table 2 is the 3-site Langmuir parameter fits for N_2 in CHA.

2. MD simulation methodology

Diffusion is simulated using Newton's equations of motion until the system properties, on average, no longer change in time. The Verlet algorithm is used for time integration. A time step of 1 fs was used in all simulations. For each simulation, *initializing* CBMC moves are used to place the molecules in the domain, minimizing the energy. Next, follows an *equilibration* stage. These are essentially the same as the production cycles, only the statistics are not yet taken into account. This removes any initial large disturbances in the system do not affect statistics. After a fixed number of initialization and equilibrium steps, the MD simulation *production* cycles start. For every cycle, the statistics for determining the mean square displacements (MSDs) are updated. The MSDs are determined for time intervals ranging from 2 fs to 1 ns. In order to do this, an order-N algorithm, as detailed in Chapter 4 of Frenkel and Smit[10] is implemented. The Nosé-Hoover thermostat is applied to all the diffusing particles.

The DLPOLY code[11] was used along with the force field implementation as described in the previous section. DL_POLY is a molecular dynamics simulation package written by W. Smith, T.R. Forester and I.T. Todorov and has been obtained from CCLRCs Daresbury Laboratory via the website[11].

The MD simulations were carried out for a variety of molecular loadings. All simulations were carried out on clusters of PCs equipped with Intel Xeon processors running at 3.4 GHz on the Linux operating system. Each MD simulation, for a specified loading, was run for 120 h, determined to be long enough to obtain reliable statistics for determination of the diffusivities. Several independent MD simulations were run and the results averaged.

The self-diffusivities, $D_{i,self}$, were computed by analyzing the mean square displacement of each component:

$$D_{i,self} = \frac{1}{2N_i} \lim_{\Delta t \to \infty} \frac{1}{\Delta t} \left\langle \left(\sum_{l=1}^{N_i} \left(\mathbf{r}_{l,i}(t+\Delta t) - \mathbf{r}_{l,i}(t) \right)^2 \right) \right\rangle \qquad (1)$$

In this expression N_i represents the number of molecules of species i respectively, and $\mathbf{r}_{l,i}(t)$ is the position of molecule l of species i at any time t. For 1D channel structures (MOR, LTL), the reported diffusivities are along the z-direction. For DDR the reported diffusivities are the averages in x- and y-directions; for DDR there is no connectivity in the z-direction. For all MFI and CHA the average values in the three coordinate directions are presented. In all cases reported here, the MSD values were linear in t and we found no evidence of single file diffusion characteristics.

3. References

[1] C. Baerlocher, L.B. McCusker, Database of Zeolite Structures, International Zeolite Association, http://www.iza-structure.org/databases/, 26 June 2001.
[2] S. Calero, D. Dubbeldam, R. Krishna, B. Smit, T.J.H. Vlugt, J.F.M. Denayer, J.A. Martens, T.L.M. Maesen, Understanding the role of sodium during adsorption. A force field for alkanes in sodium exchanged faujasites, J. Am. Chem. Soc. 126 (2004) 11377-11386.
[3] J.P. Ryckaert, A. Bellemans, Molecular dynamics of liquid alkanes, Faraday Discuss. Chem. Soc. 66 (1978) 95-106.
[4] D. Dubbeldam, S. Calero, T.J.H. Vlugt, R. Krishna, T.L.M. Maesen, B. Smit, United Atom Forcefield for Alkanes in Nanoporous Materials, J. Phys. Chem. B 108 (2004) 12301-12313.
[5] J.G. Harris, K.H. Yung, Carbon Dioxide's Liquid-Vapor Coexistence Curve And Critical Properties as Predicted by a Simple Molecular Model, J. Phys. Chem. 99 (1995) 12021-12024.
[6] K. Makrodimitris, G.K. Papadopoulos, D.N. Theodorou, Prediction of permeation properties of CO_2 and N_2 through silicalite via molecular simulations, J. Phys. Chem. B 105 (2001) 777-788.
[7] E. García-Pérez, J.B. Parra, C.O. Ania, J.M. Van Baten, R. Krishna, S. Calero, A computational study of CO_2, N_2 and CH_4 adsorption in zeolites, The Sixth International Symposium Effects of Surface Heterogeneity in Adsorption and Catalysis on Solids, Zacopane, Poland, 2006.
[8] T.J.H. Vlugt, R. Krishna, B. Smit, Molecular simulations of adsorption isotherms for linear and branched alkanes and their mixtures in silicalite, J. Phys. Chem. B 103 (1999) 1102-1118.
[9] T.J.H. Vlugt, BIGMAC, University of Amsterdam, http://molsim.chem.uva.nl/bigmac/, 1 November 2000.
[10] D. Frenkel, B. Smit, Understanding molecular simulations: from algorithms to applications, Academic Press, 2nd Edition, San Diego, 2002.

[11]   W. Smith, T.R. Forester, I.T. Todorov, The DL_POLY Molecular Simulation Package, Warrington, England, http://www.cse.clrc.ac.uk/msi/software/DL_POLY/index.shtml, March 2006.

Table 1. Summary of force field used in GCMC and MD simulations

The interaction between adsorbates was calculated using Lennard-Jones potentials and electrostatic interactions using an Ewald summation method. For adsorbate-adsorbate interactions, Lorentz-Berthelot mixing rules were applied for σ and ε/k_B. Leonard-Jones interaction with the zeolite was only taken σ and ε/k_B and epsilon for the adsorbates and for the interaction with the adsorbates and with the zeolites. The charges are also shown for the pseudo atoms.

(pseudo-) atom	Atom-atom σ / Å	Atom-atom ε/k_B / K	Atom - O in zeolite σ / Å	Atom - O in zeolite ε/k_B / K	charge
CH_4	3.72	158.5	3.47	115	0
C (CO_2)	2.757	28.129	2.7815	50.2	0.6512
O (CO_2)	3.033	80.507	2.9195	84.93	-0.3256
N (N_2)	3.32	36.4	3.06	58.25	-0.40484

The molecule geometries were fixed. The bond angle for CO_2 is 180°. For N_2, a point charge is located in the middle between the two atoms, that is –2 the magnitude of the charges on N, so that the total molecule charge is zero. The following table shows the bond lengths that were used:

bond	bond length / Å
N-N (N_2)	1.098
C-O (CO_2)	1.16

The zeolite atoms are considered immobile. The following table shows the charges used for the zeolite atoms:

atom	charge
$O_{Zeolite}$	-1.025
$Si_{Zeolite}$	2.05

Table 2. Three-site Langmuir parameters for CH_4 and CO_2 in MFI, CHA and DDR. The saturation capacity q_{sat} has the units of mol kg^{-1}. The Langmuir parameters b_i, have the units of Pa^{-1}.

Zeolite	Molecule, Temperature	Three-Site Langmuir parameters					
		$b_{i,A}$	$q_{i,sat,A}$	$b_{i,B}$	$q_{i,sat,B}$	$b_{i,C}$	$q_{i,sat,C}$
MFI	CH_4, 300 K	3.25×10^{-6}	2.8	2.2×10^{-8}	0.7	1.12×10^{-10}	0.5
CHA	CH_4, 300 K	1.72×10^{-6}	2.77	2.7×10^{-8}	4.16	9.0×10^{-10}	1.39
DDR	CH_4, 300 K	3.5×10^{-6}	1.66	1.45×10^{-8}	1.66	2.7×10^{-11}	0.83
MFI	CO_2, 300 K	5.78×10^{-6}	3.4	2.76×10^{-8}	1.0	1.46×10^{-9}	1.5
CHA	CO_2, 300 K	5.21×10^{-6}	6.93	1.02×10^{-7}	1.73	1.17×10^{-9}	1.73
DDR	CO_2, 300 K	7.5×10^{-6}	1.66	2.0×10^{-6}	1.66	1.2×10^{-8}	1.25
CHA	N_2, 300 K	2.5×10^{-7}	4.58	6.86×10^{-9}	3.47	1.35×10^{-11}	1.66

Appendix A2

GCMC simulation results for adsorption of CH_4, CO_2 and N_2 in different zeolite structures

AFI, 300 K, pure
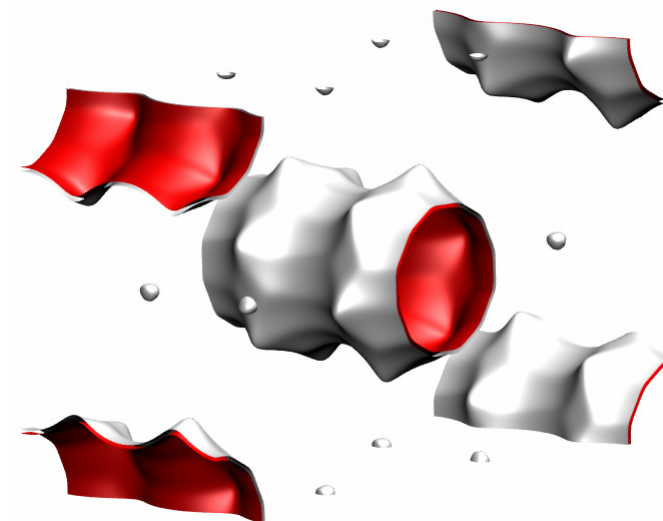
CO₂
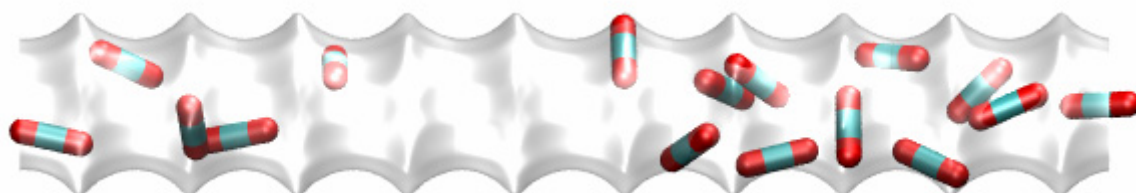
f_i=1000 kPa
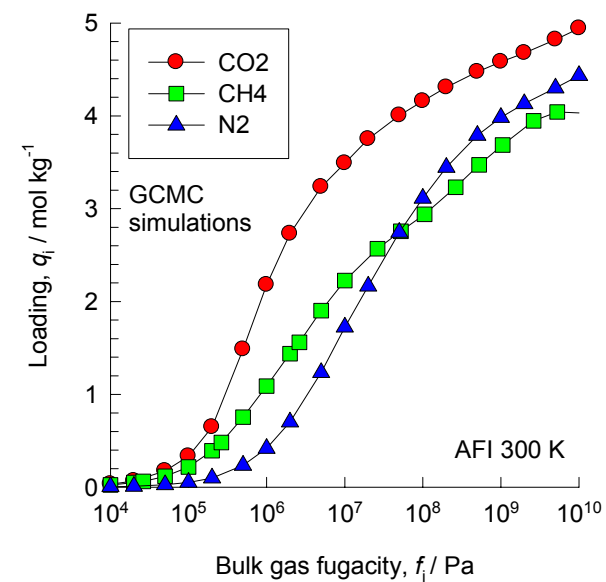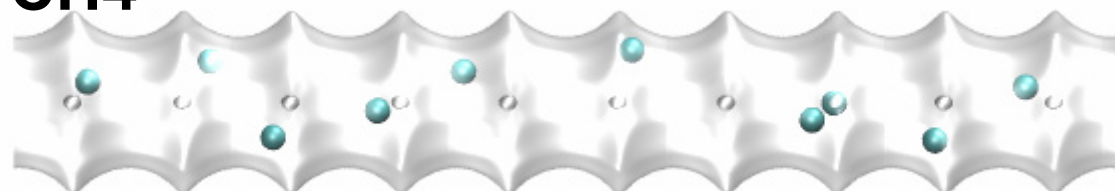
CH4

AFI, 300 K, mixture

$$f_{CO2} = 500 \text{ kPa}; \quad f_{CH4} = 9500 \text{ kPa}$$

ternary

Legend: CH4, CO2, N2

GCMC simulations; $f_1 = f_2 = f_3$

AFI 300 K

Loading, q_i / mol kg^{-1}

partial gas phase fugacity, f_i / Pa

binary

Legend: CO2, CH4

GCMC simulations; $f_1 = f_2$

AFI 300 K

Loading, q_i / mol kg^{-1}

partial gas phase fugacity, f_i / Pa

TON, 300 K, pure

CO$_2$

f_i=1000 kPa

CH4

GCMC simulations
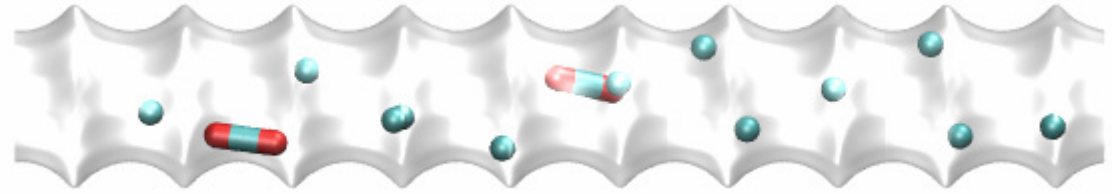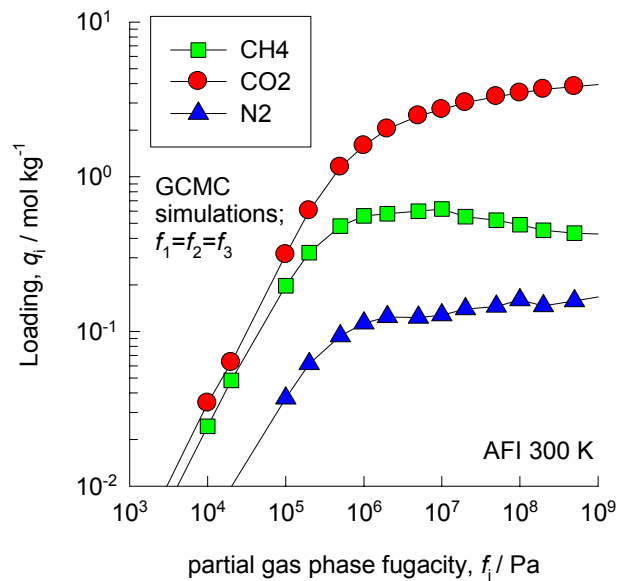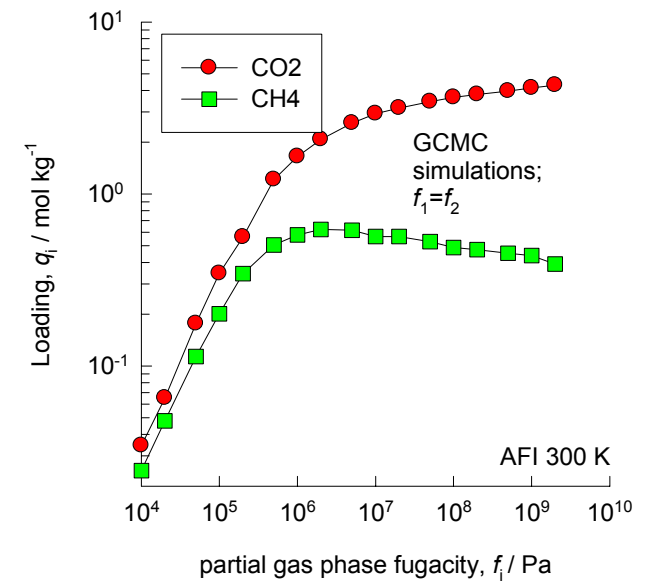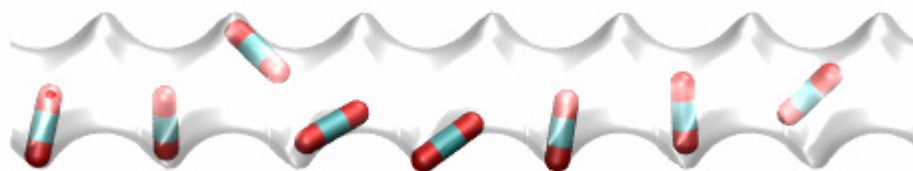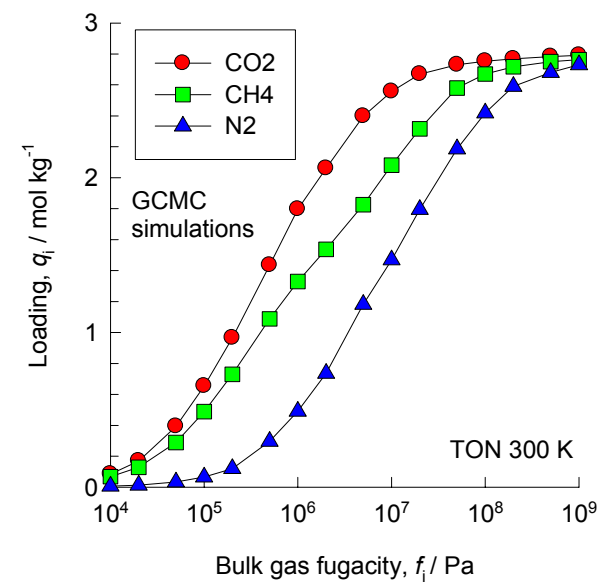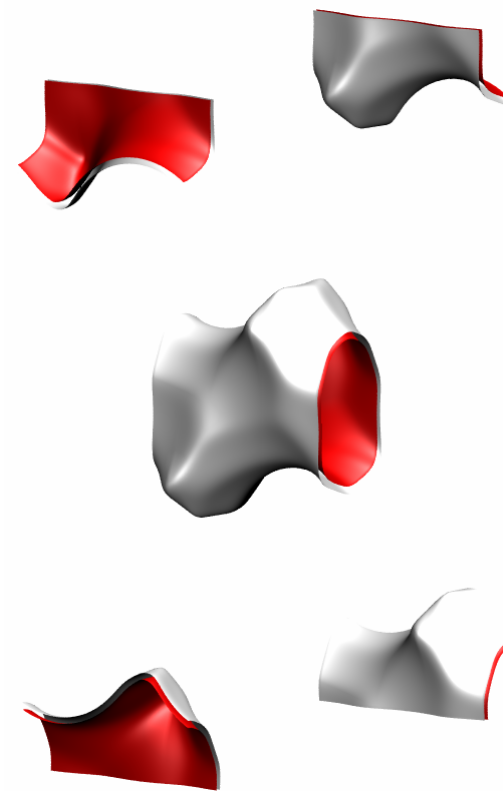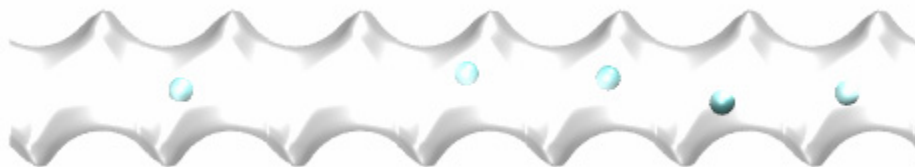
TON 300 K

TON, 300 K, mixture

$f_{CO2} = 500$ kPa; $f_{CH4} = 9500$ kPa
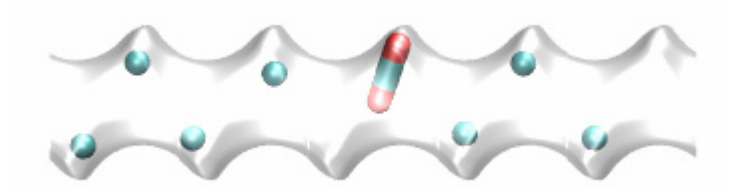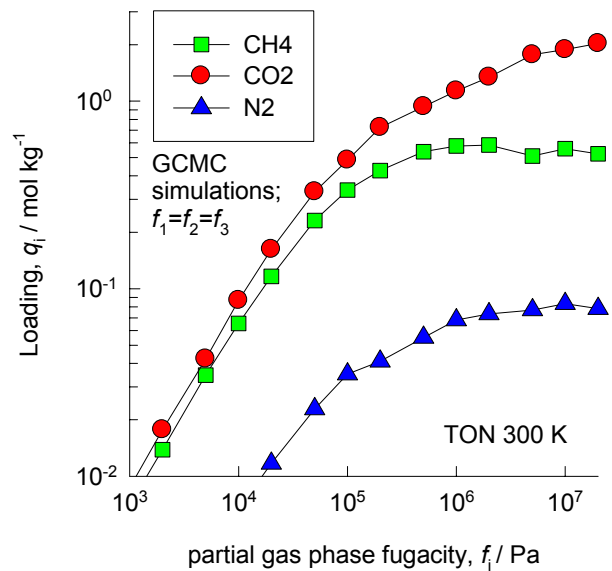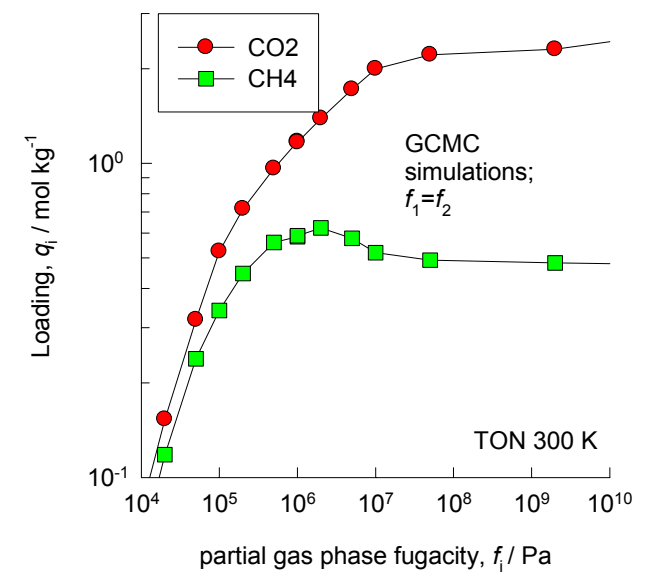
ternary

binary

FER, 300 K, pure
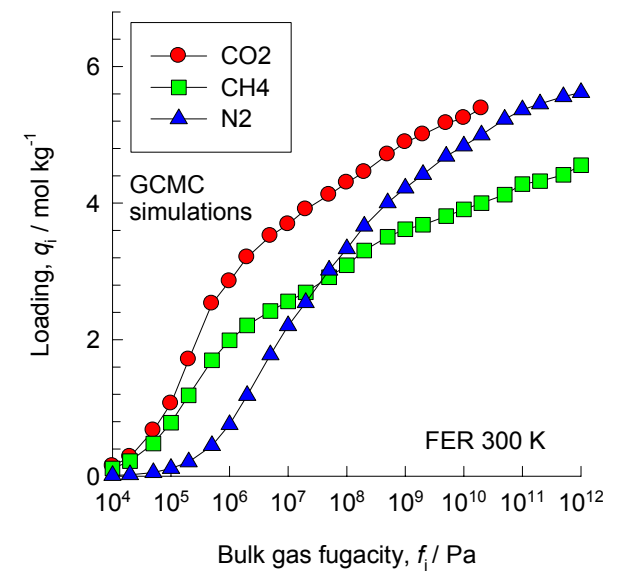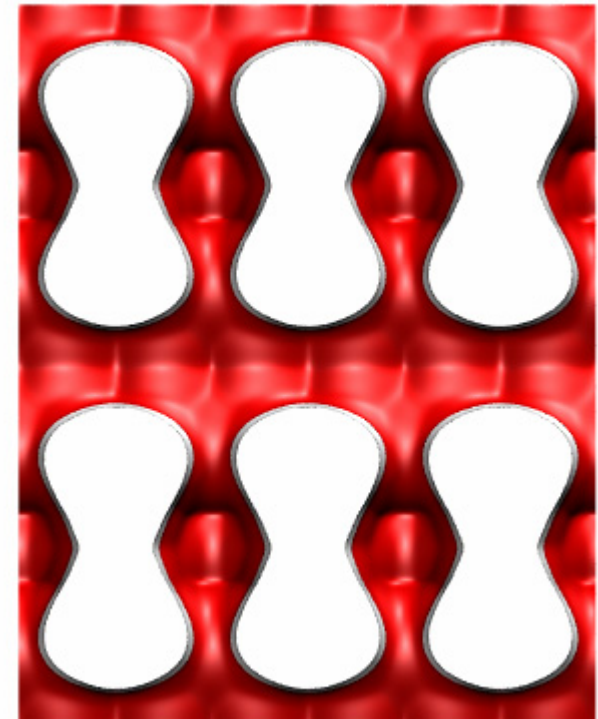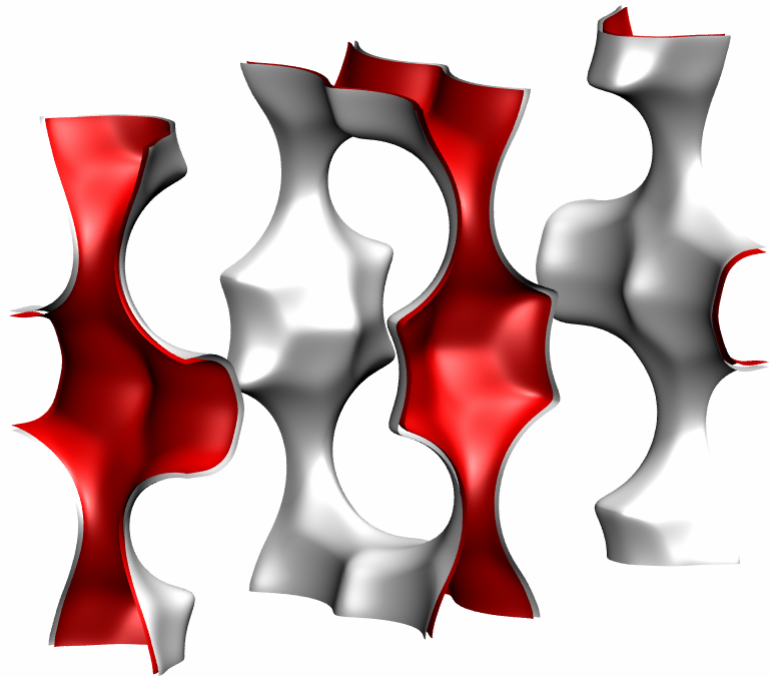
FER, 300 K, pure

CO_2
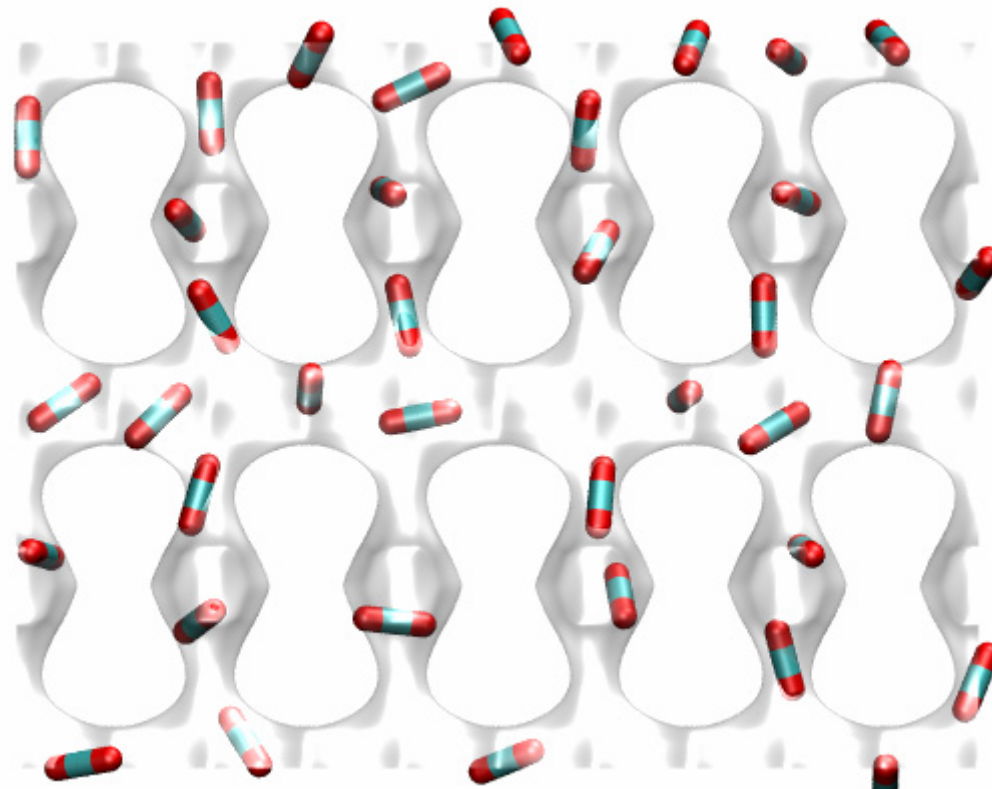
f_i=1000 kPa

CH4

FER, 300 K, mixture

$f_{CO2} = 500$ kPa;
$f_{CH4} = 9500$ kPa

ternary

GCMC simulations; $f_1 = f_2 = f_3$

FER 300 K

Loading, q_i / mol kg^{-1}

partial gas phase fugacity, f_i / Pa

binary

GCMC simulations; $f_1 = f_2$

FER 300 K

Loading, q_i / mol kg^{-1}

partial gas phase fugacity, f_i / Pa

MOR, 300 K, pure

GCMC simulations

MOR 300 K

- CO2
- CH4
- N2

MOR, 300 K, pure

CO$_2$

CO$_2$
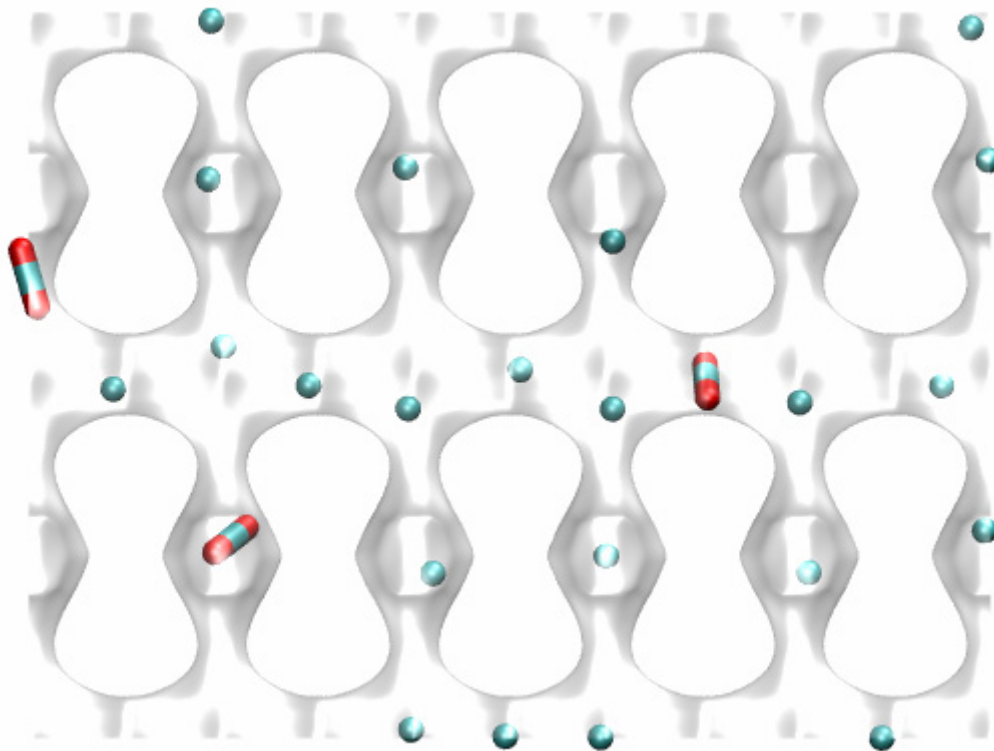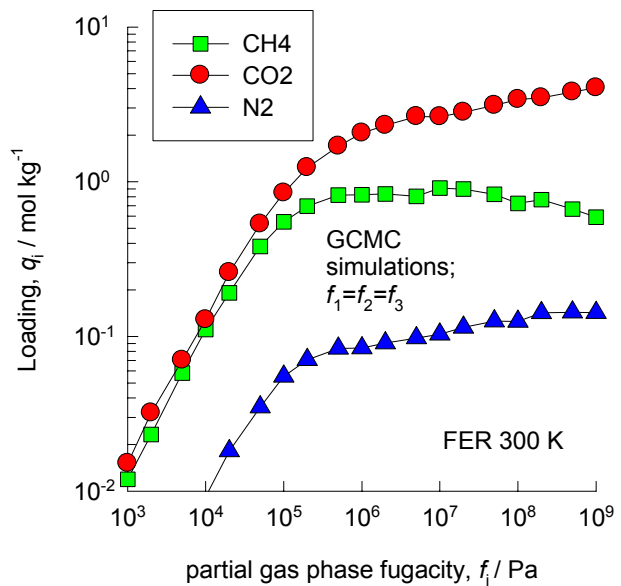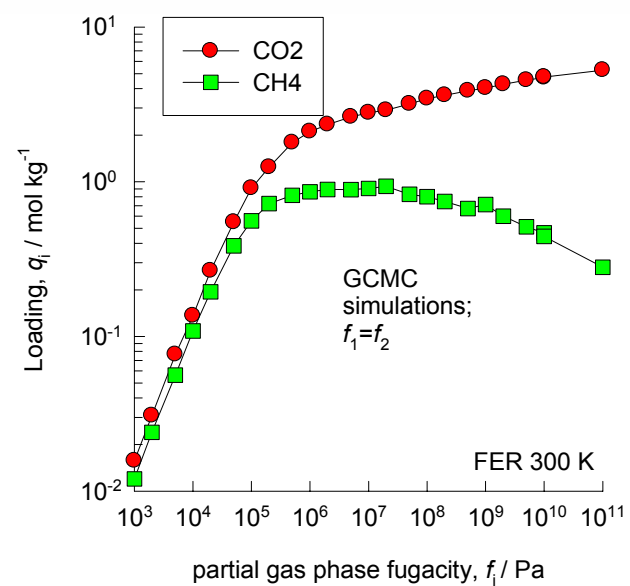
f_i=1000 kPa

f_i=10 kPa

CH4

MOR, 300 K, mixture

$f_{CO2} = 500$ kPa;
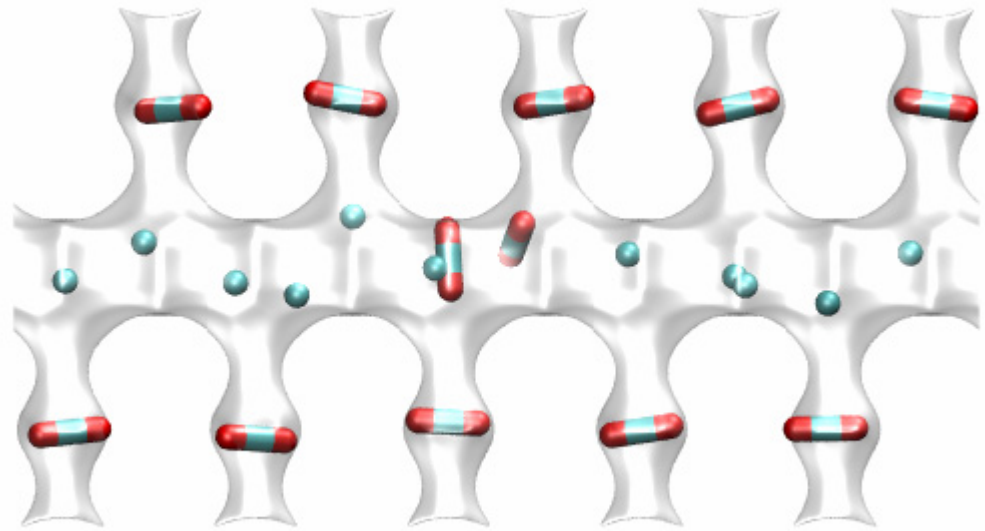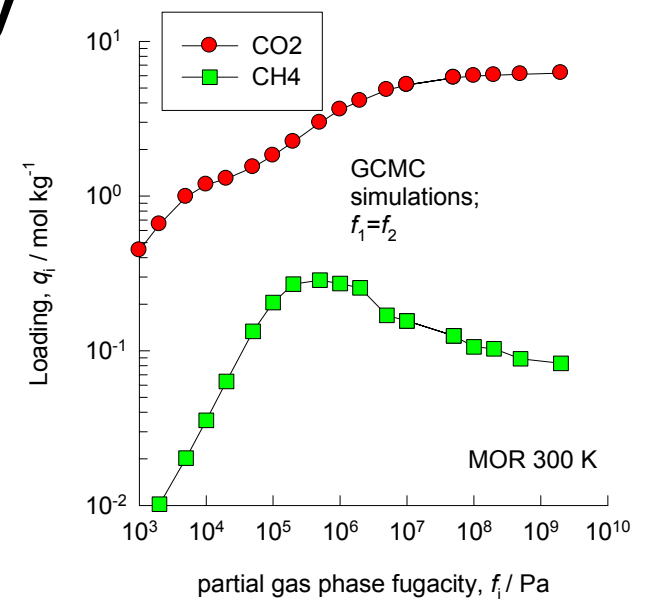
$f_{CH4} = 9500$ kPa

ternary

binary

MOR, 300 K, self diffusivities

CH4
CO2

self diffusivity / 10^{-8} m^2 s^{-1}

Total loading, q / mol kg^{-1}

MD simulations;
pure components;
MOR; 300 K

CH4
CO2

self diffusivity / 10^{-8} m^2 s^{-1}

Total mixture loading, q / mol kg^{-1}

MD simulations;
binary mixture;
MOR; 300 K;
$q_1 = q_2$

MOR, 300 K, diffusion selectivities

1:1 mixture
pure components

CO_2/CH_4 diffusion selectivity

Total loading, q / mol kg^{-1}

MD simulations
of self-diffusivities
in pure components
and binary mixtures
in MOR at 300 K

LTL, 300 K, pure

CO₂

f_i=1000 kPa

CH4

GCMC simulations

LTL 300 K

Loading, q_i / mol kg^{-1}

Bulk gas fugacity, f_i / Pa

- CO2
- CH4
- N2

LTL, 300 K, mixture

f_{CO2} = 500 kPa; f_{CH4} = 9500 kPa
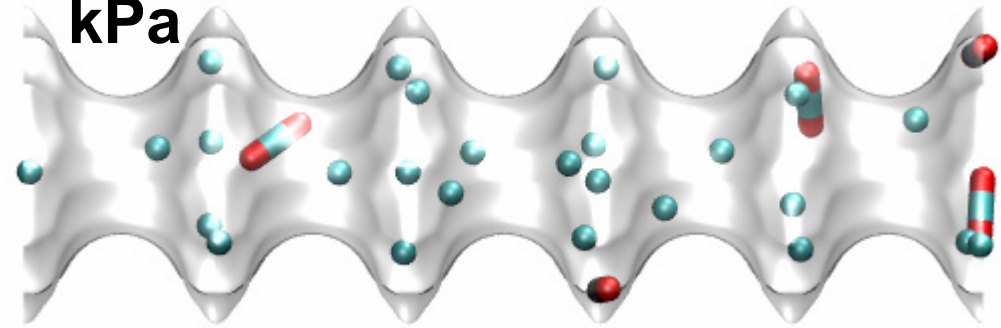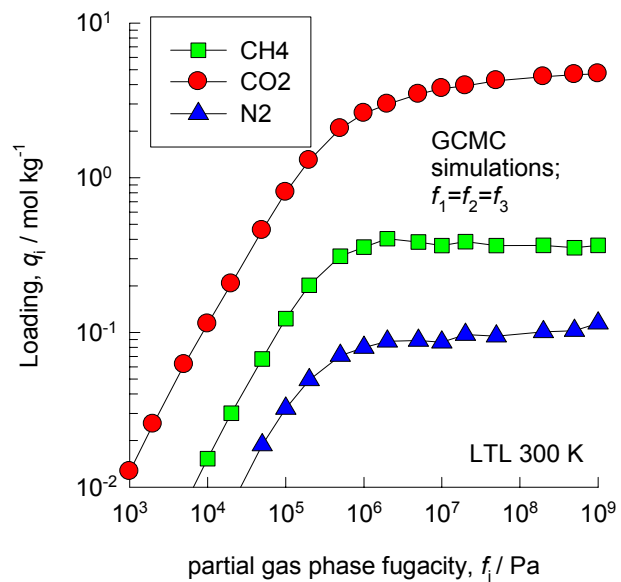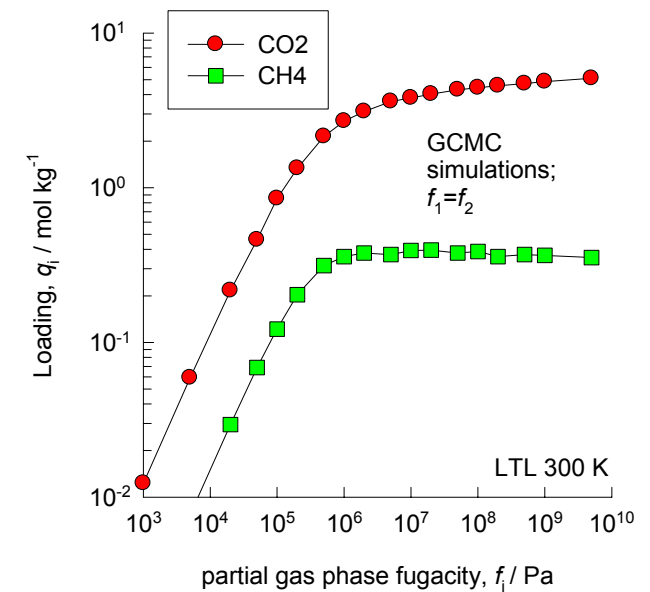
ternary

binary

LTL, 300 K, self diffusivities
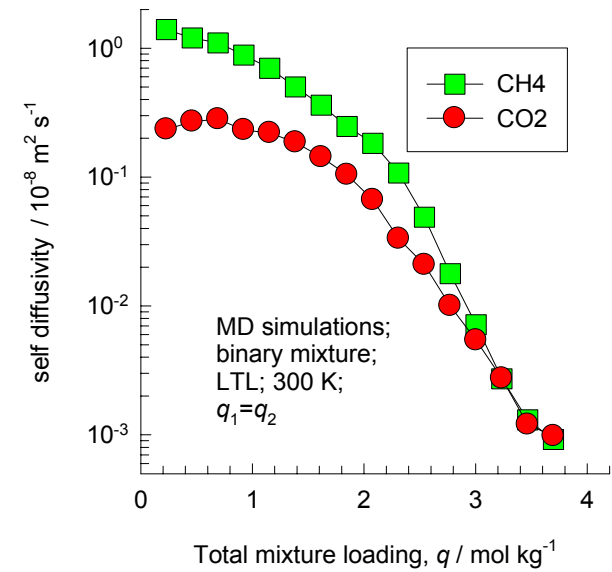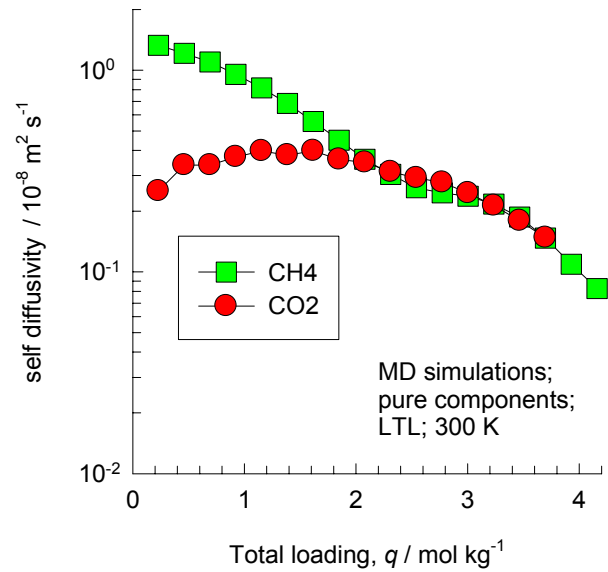
LTL, 300 K, diffusion selectivities
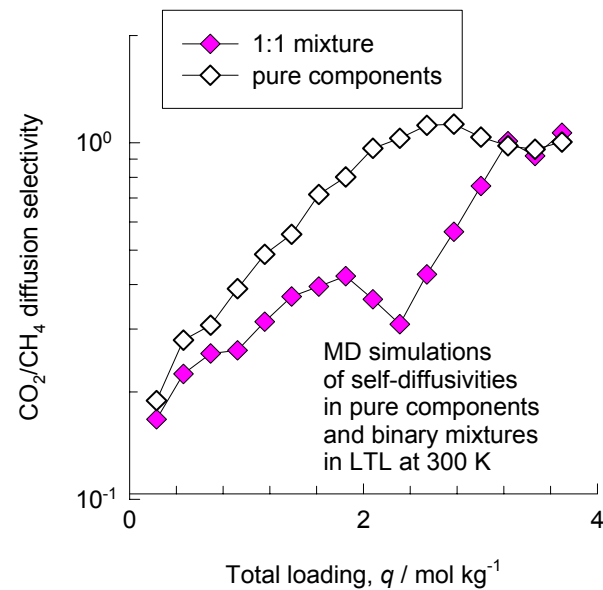
MFI, 300 K, pure
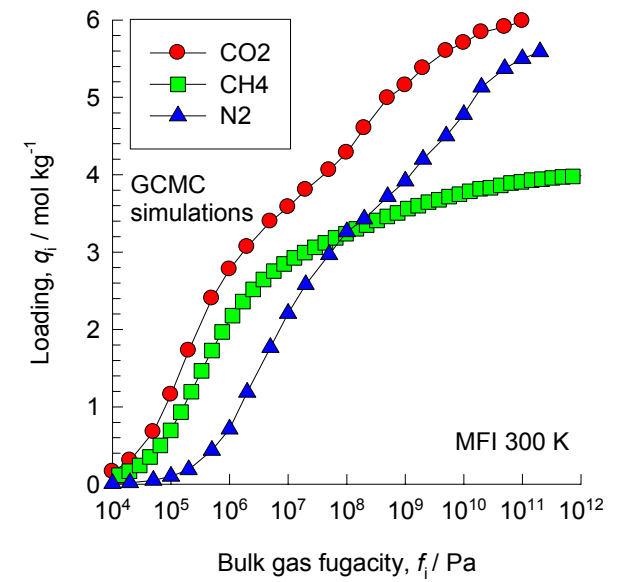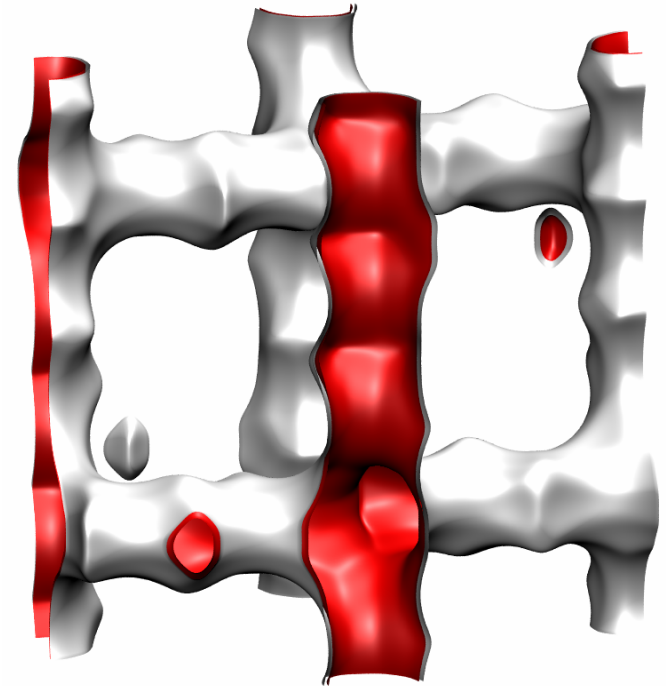
MFI, 300 K, pure
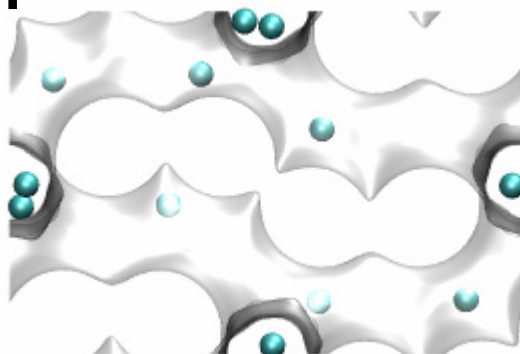
CH4   CO$_2$
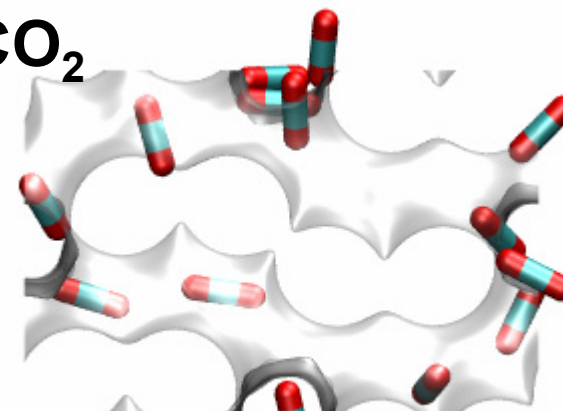
f_i=1000 kPa
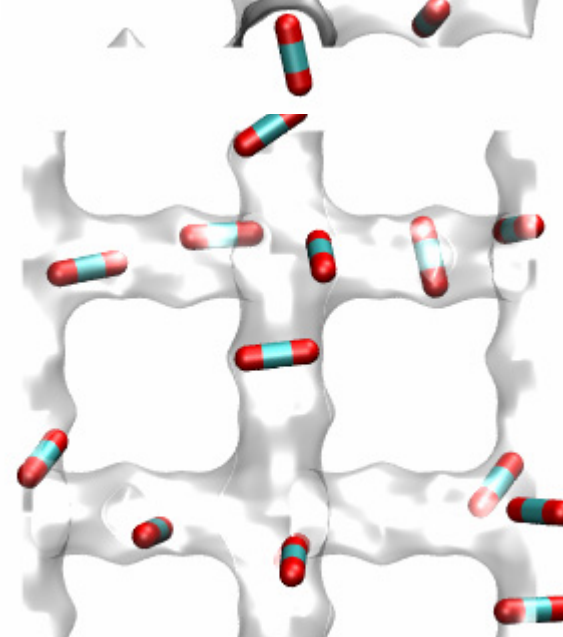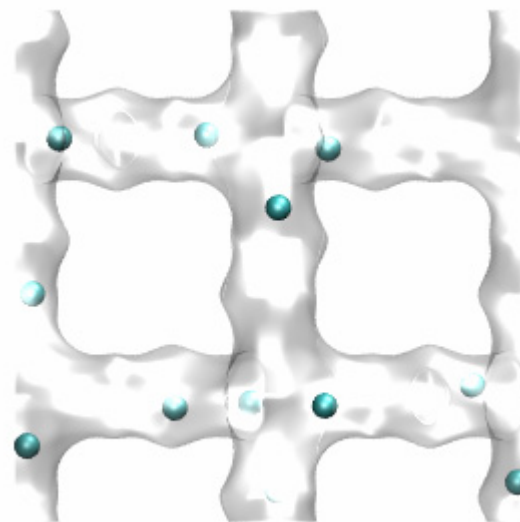
MFI, 300 K, mixture
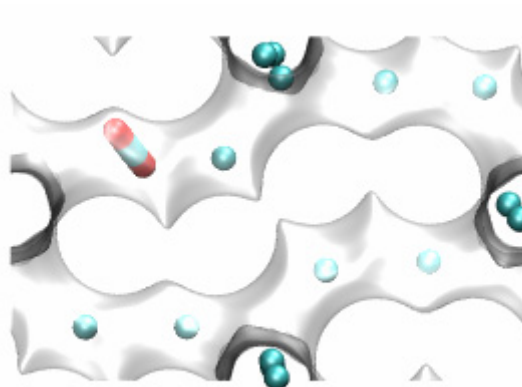
f_{CO2} = 500 kPa;
f_{CH4} = 9500 kPa
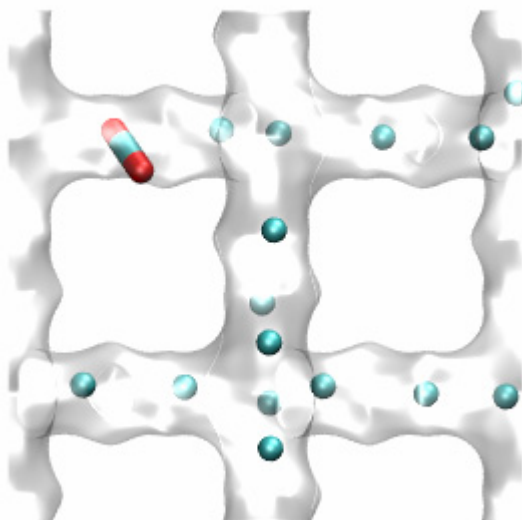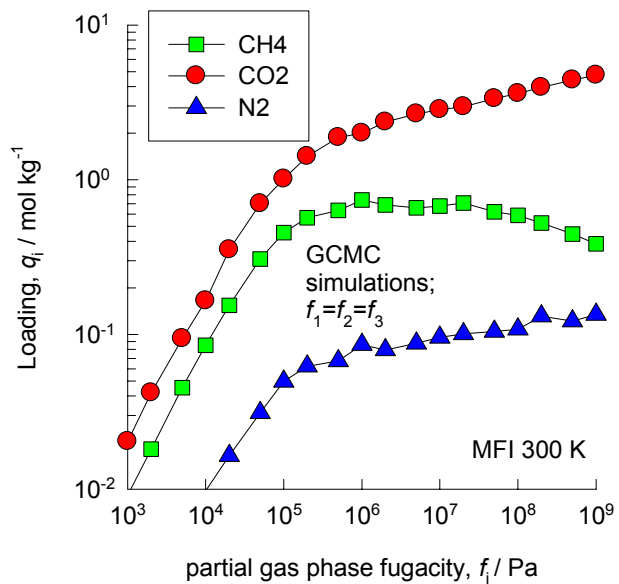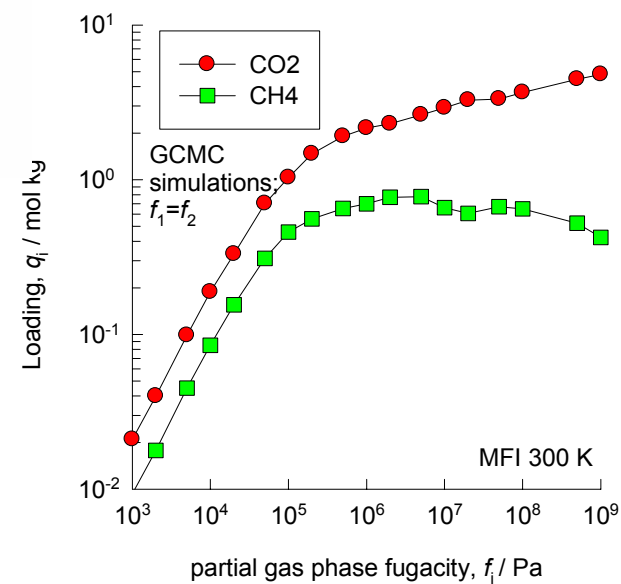
ternary

binary

MFI, 300 K, self diffusivities
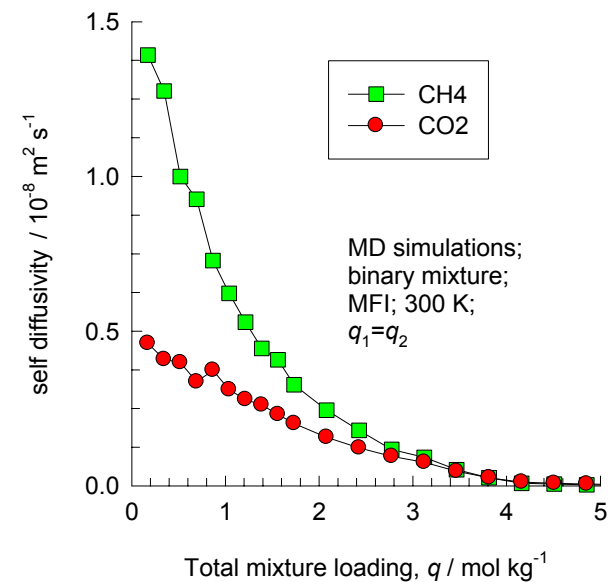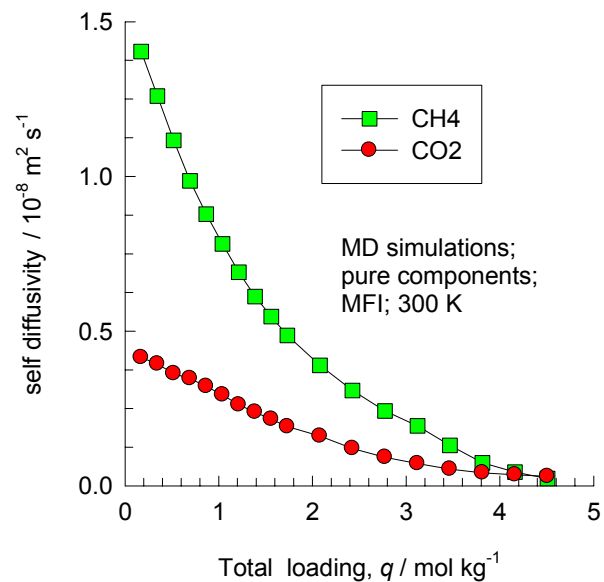
MFI, 300 K, diffusion selectivities
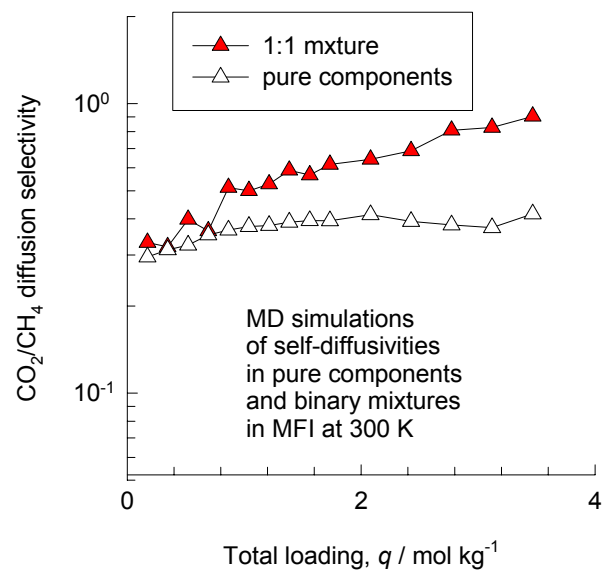
ISV, 300 K, pure
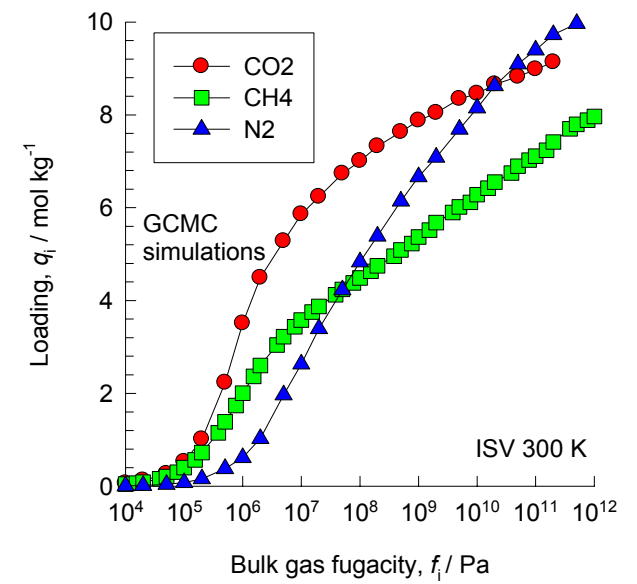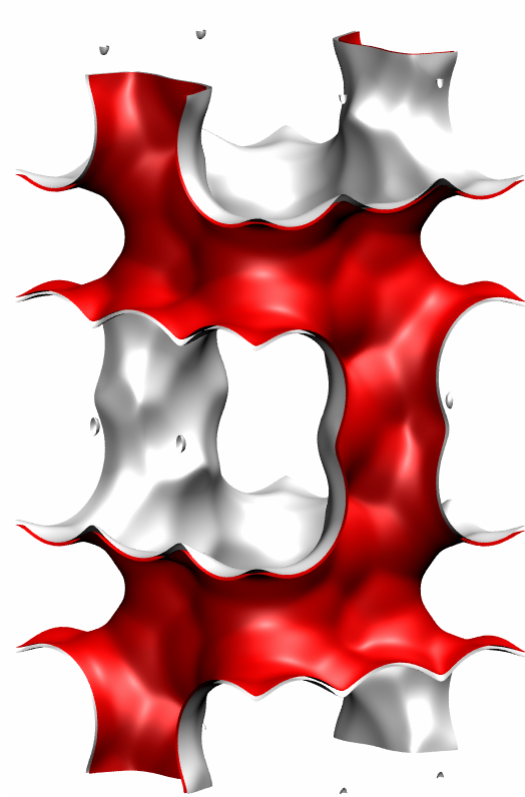
ISV, 300 K, pure

CO$_2$
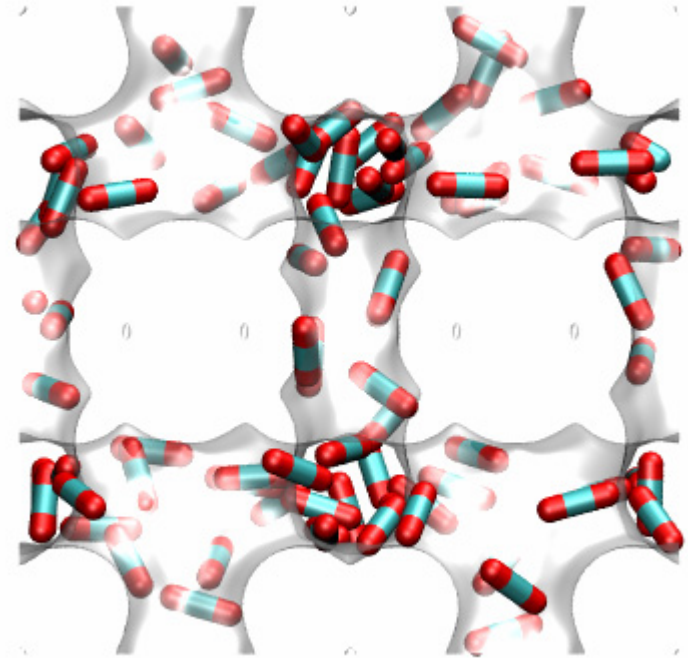
f_i=1000 kPa

CH4
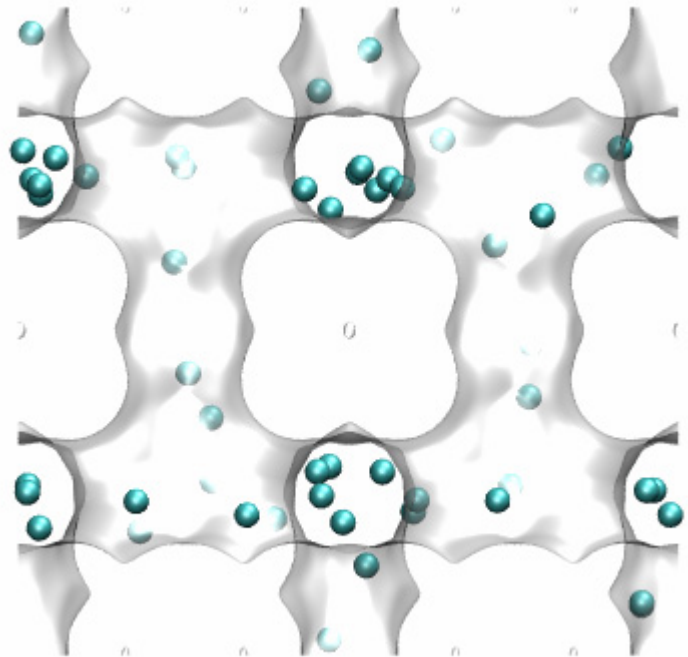
ISV, 300 K, mixture
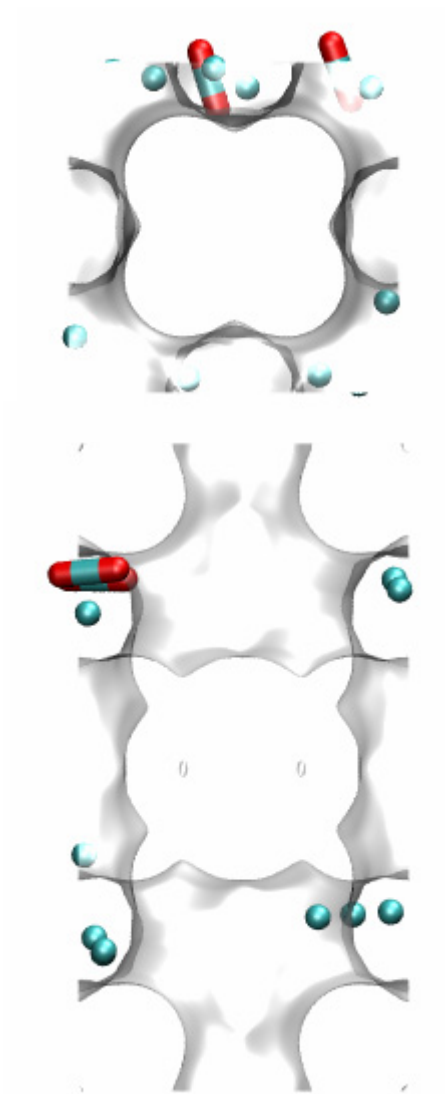
$f_{CO2}=$ 500 kPa;

f_{CH4} = 9500 kPa
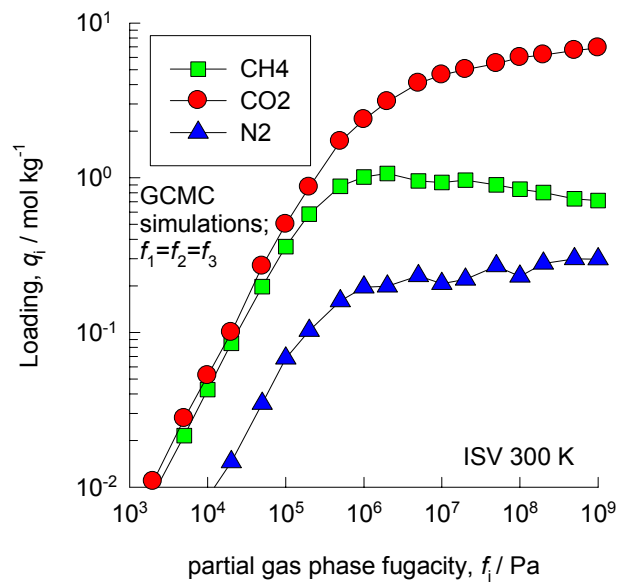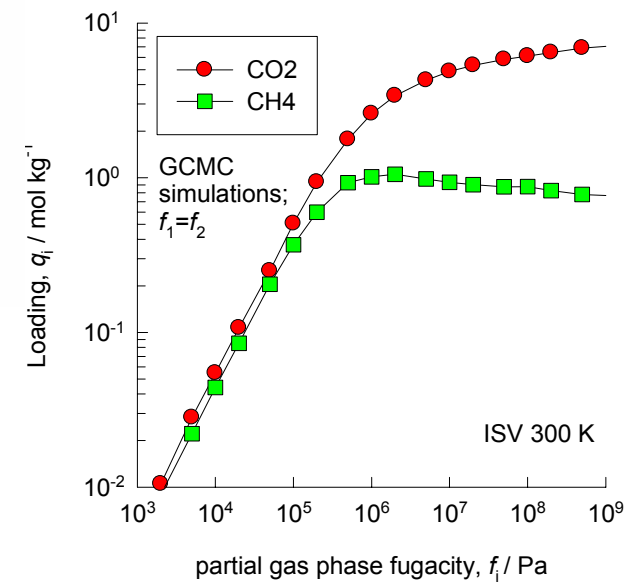
ternary

binary

BEA, 300 K, pure

CO$_2$

CH4

f_i=1000 kPa

GCMC simulations

BEA 300 K

Loading, q_i / mol kg^{-1}

Bulk gas fugacity, f_i / Pa

- CO2
- CH4
- N2
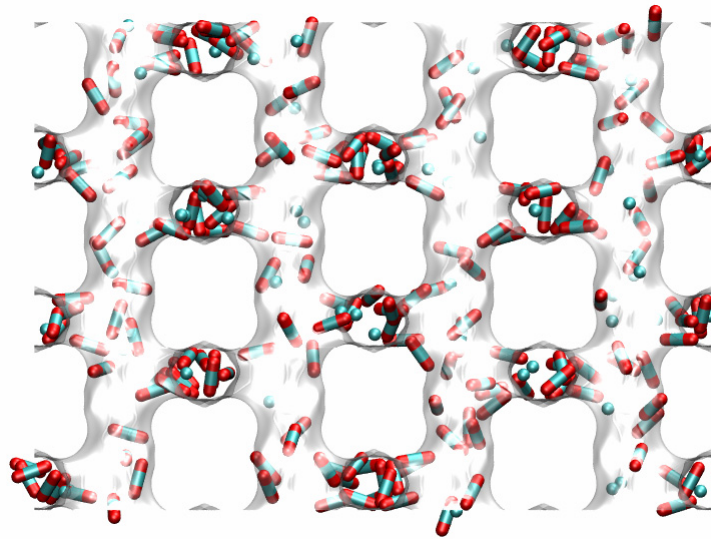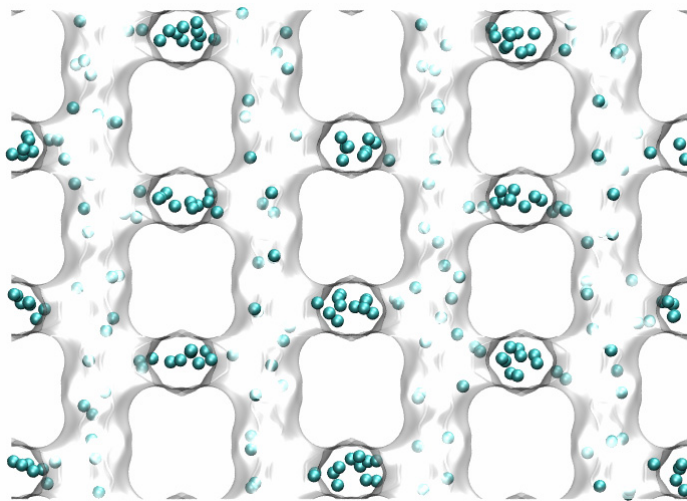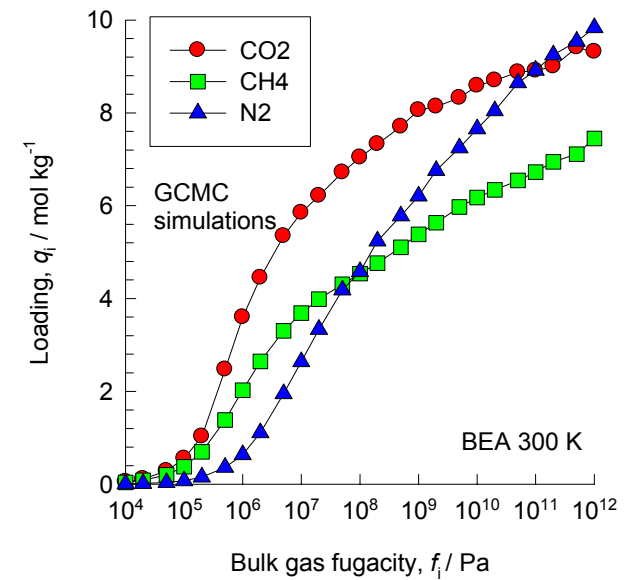
BEA, 300 K, mixture

f_{CO2} = 500 kPa;
f_{CH4} = 9500 kPa
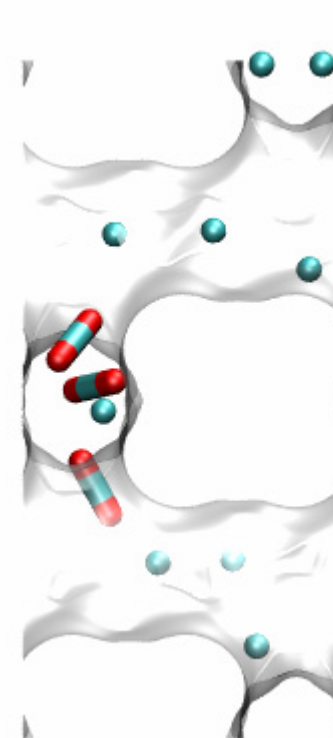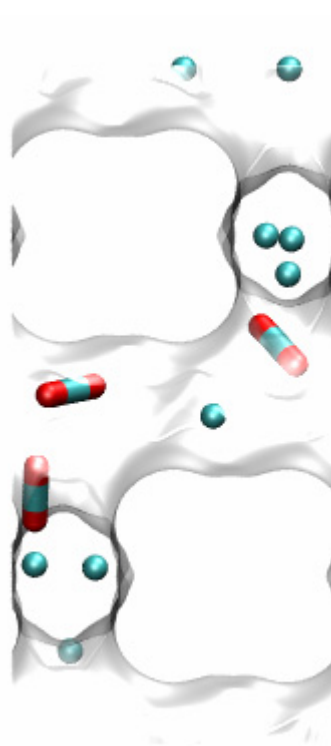
ternary

binary

LTA, 300 K, pure

GCMC simulations

LTA 300 K

Loading, q_i / mol kg^{-1}

Bulk gas fugacity, f_i / Pa

- CO2
- CH4
- N2
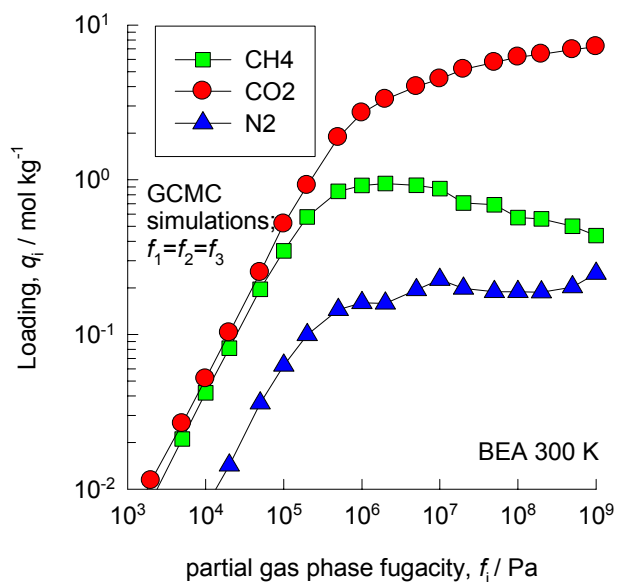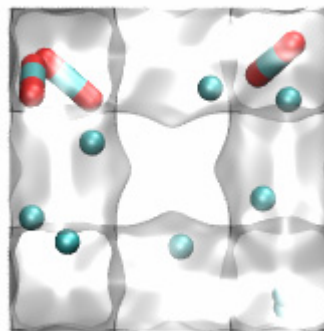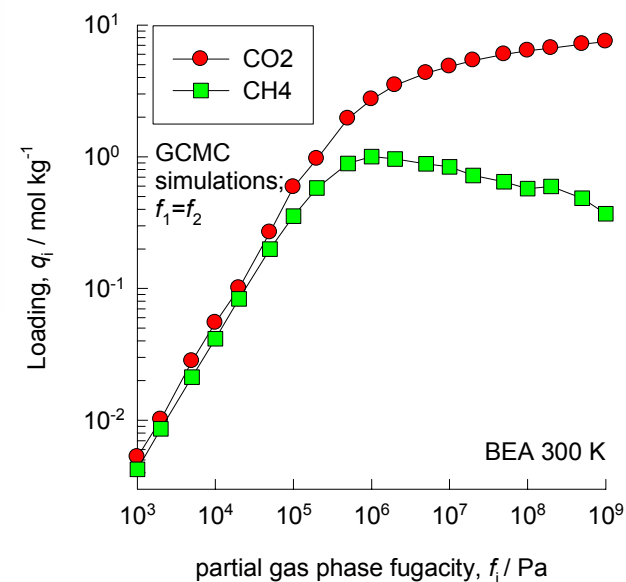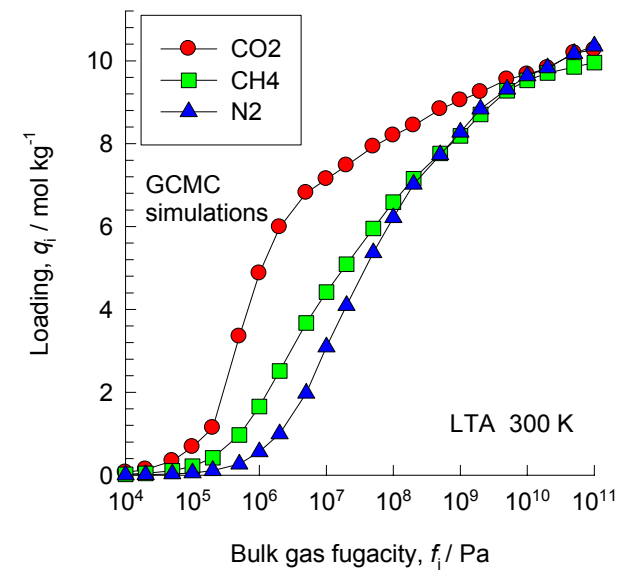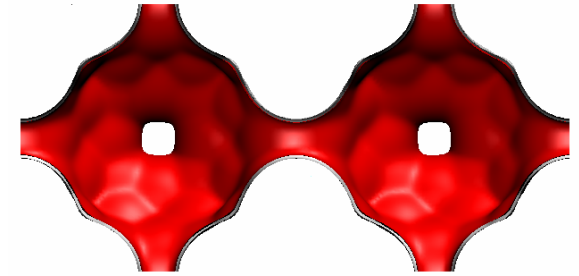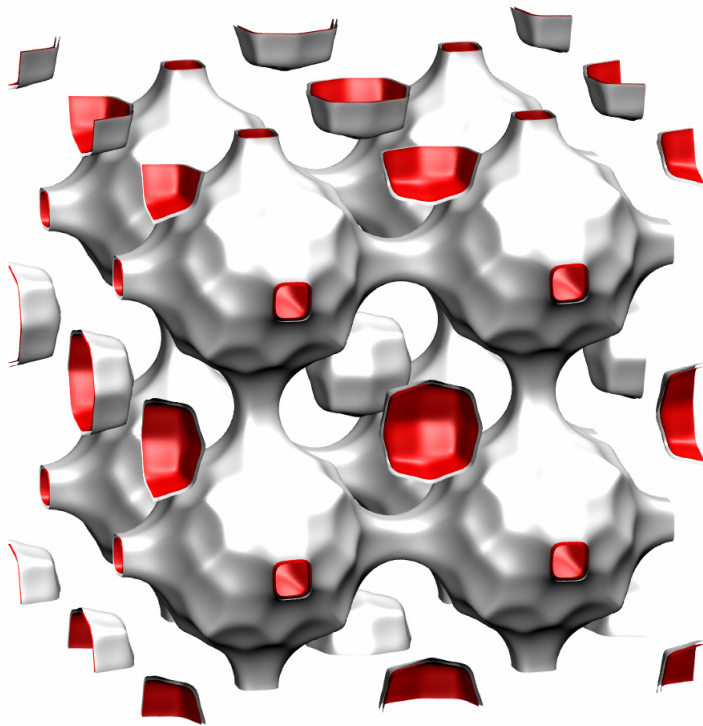
LTA, 300 K, pure

CO_2
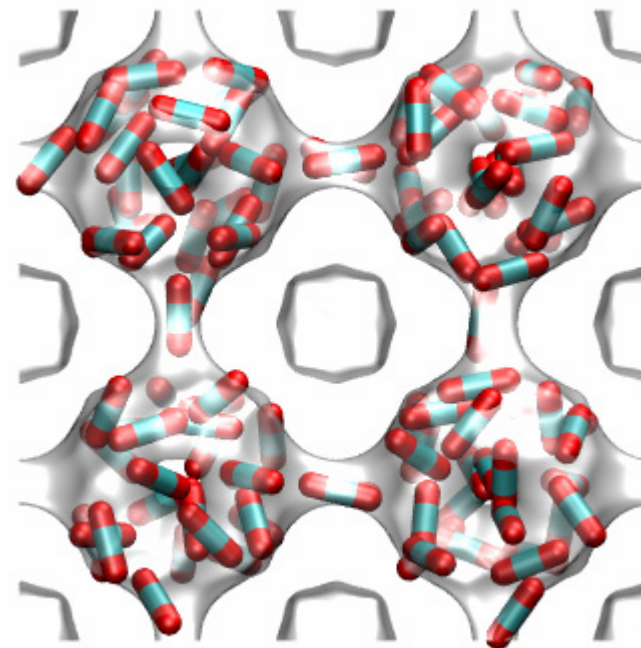
$f_i = 1000$ kPa

CH4
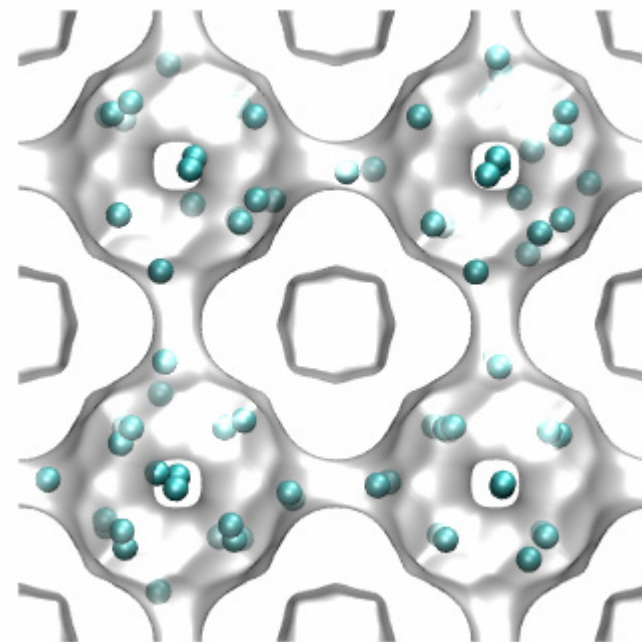
LTA, 300 K, mixture

$f_{CO2} = 500 \text{ kPa};$
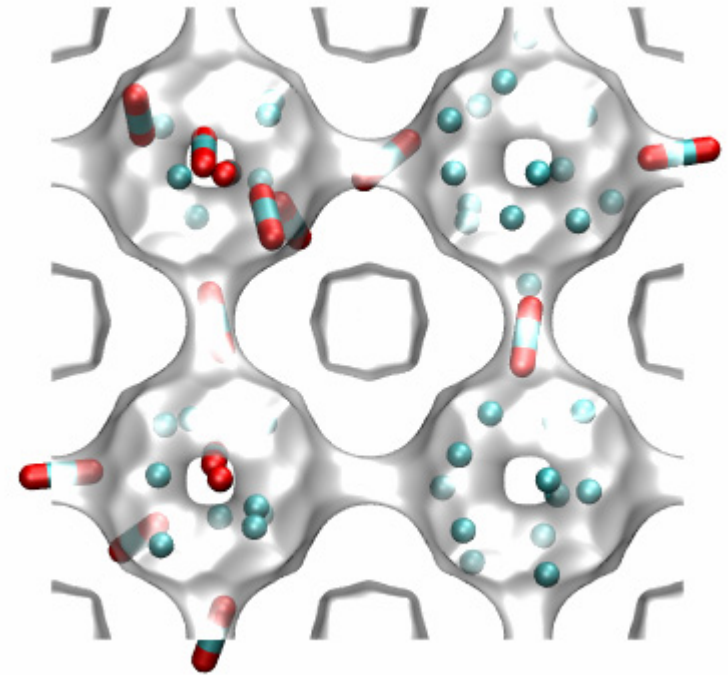
$f_{CH4} = 9500 \text{ kPa}$
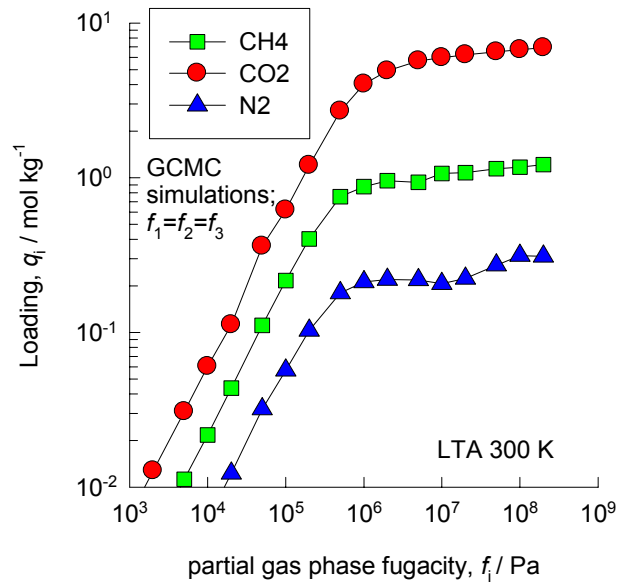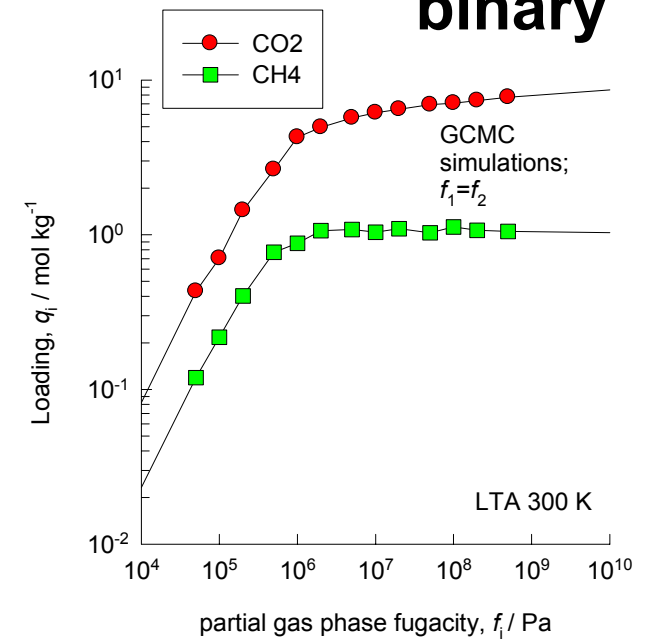
ternary

binary

FAU, 300 K, pure

CH4

f_i=1000 MPa

CO$_2$

f_i=10 MPa

GCMC simulations

FAU 300 K

Loading, q_i / mol kg^{-1}

Bulk gas fugacity, f_i / Pa

- CO2
- CH4
- N2
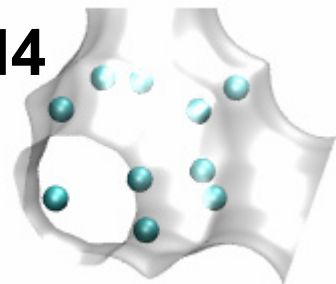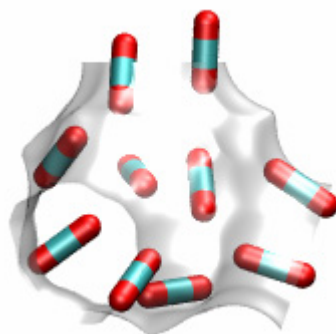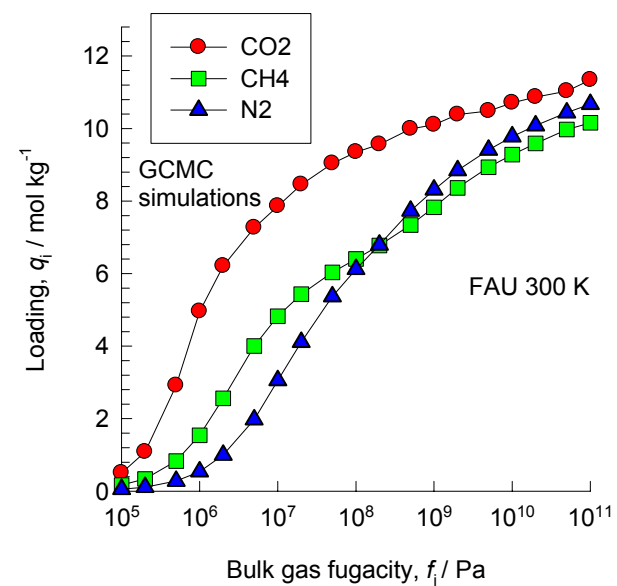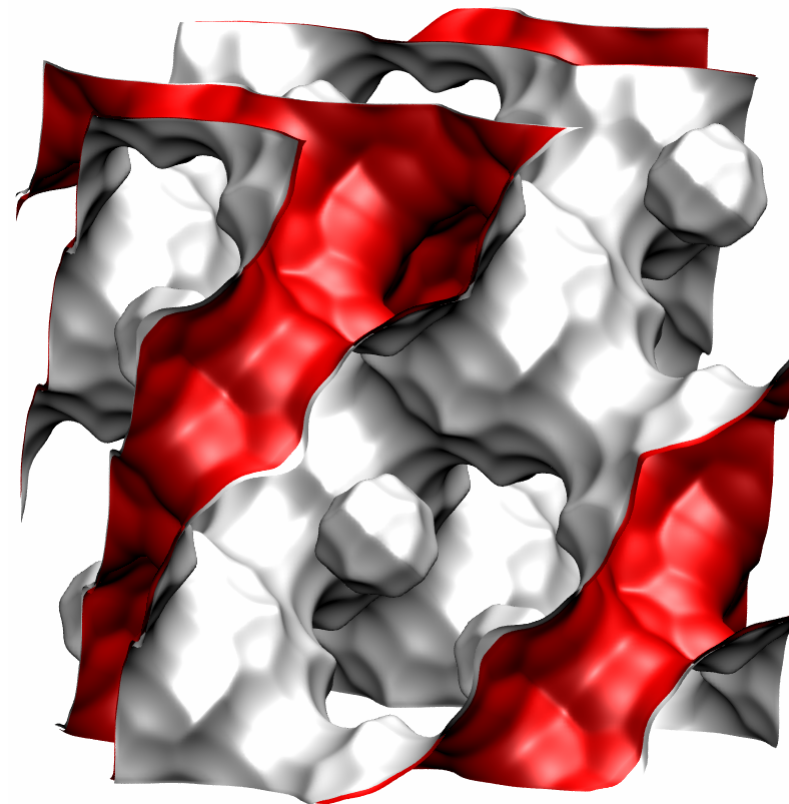
FAU, 300 K, mixture

f_{CO2} = 500 kPa;
f_{CH4} = 9500 kPa
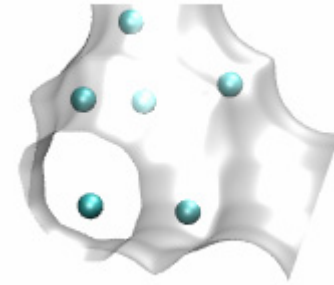
f_{CO2} = 500 kPa;
f_{CH4} = 500 kPa
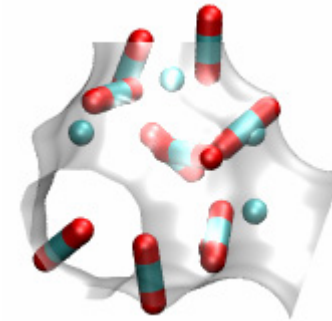
ternary

binary

CHA, 300 K, pure

GCMC simulations

- ● CO2
- ■ CH4
- ▲ N2

CHA 300 K

Loading, q_i / mol kg^{-1}

Bulk gas fugacity, f_i / Pa
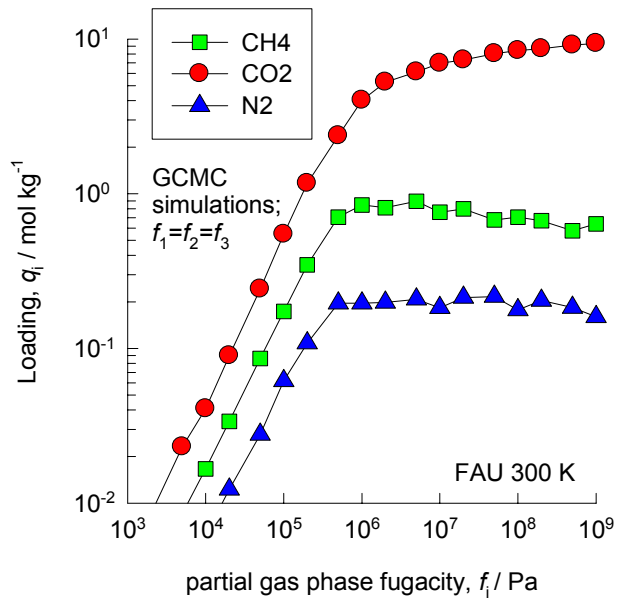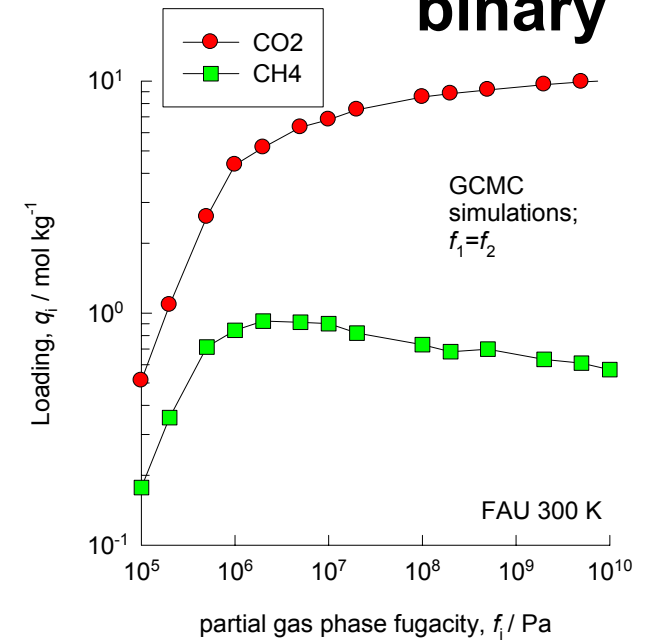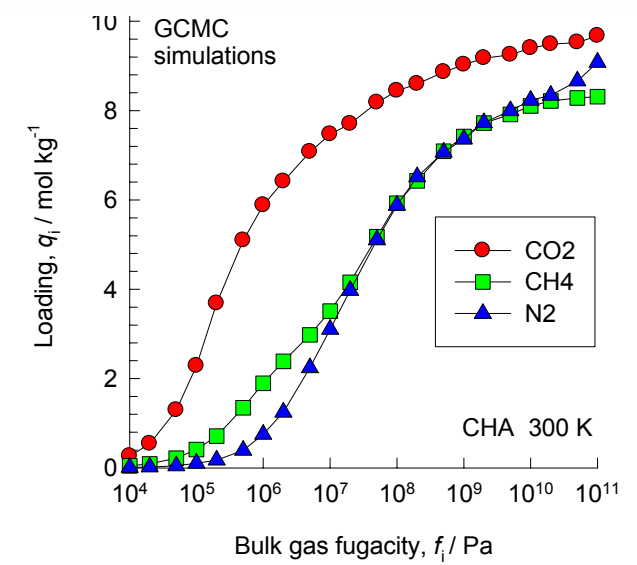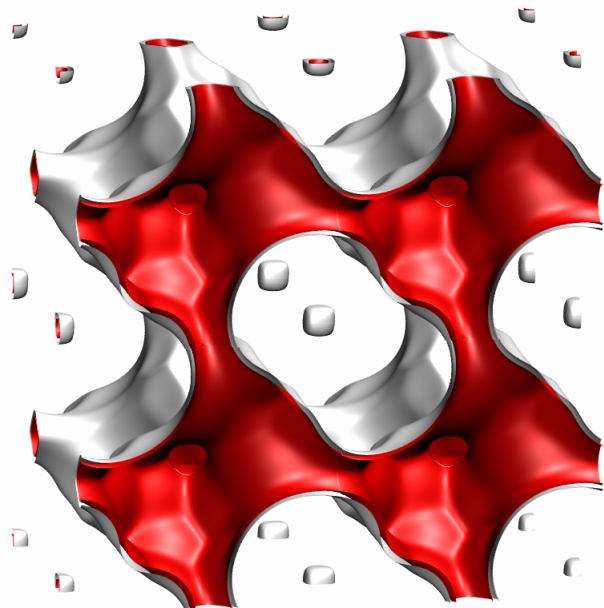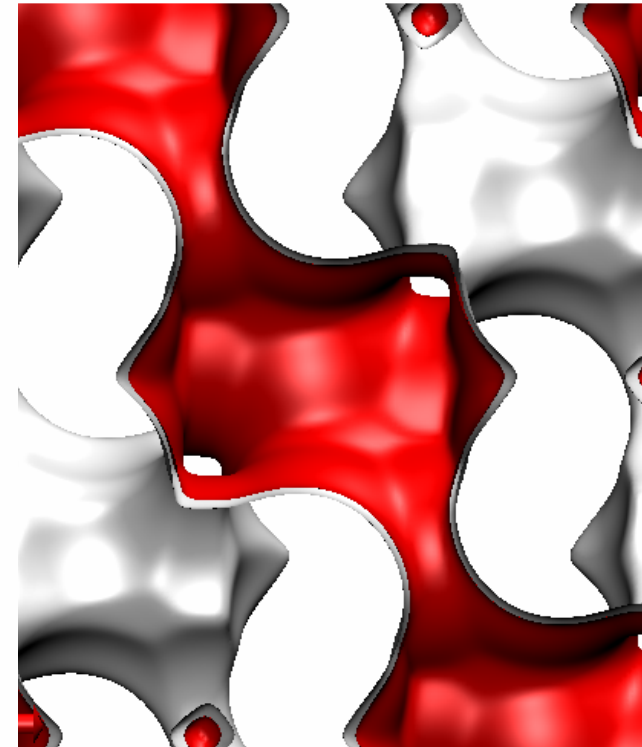
CHA, 300 K, pure

CH4
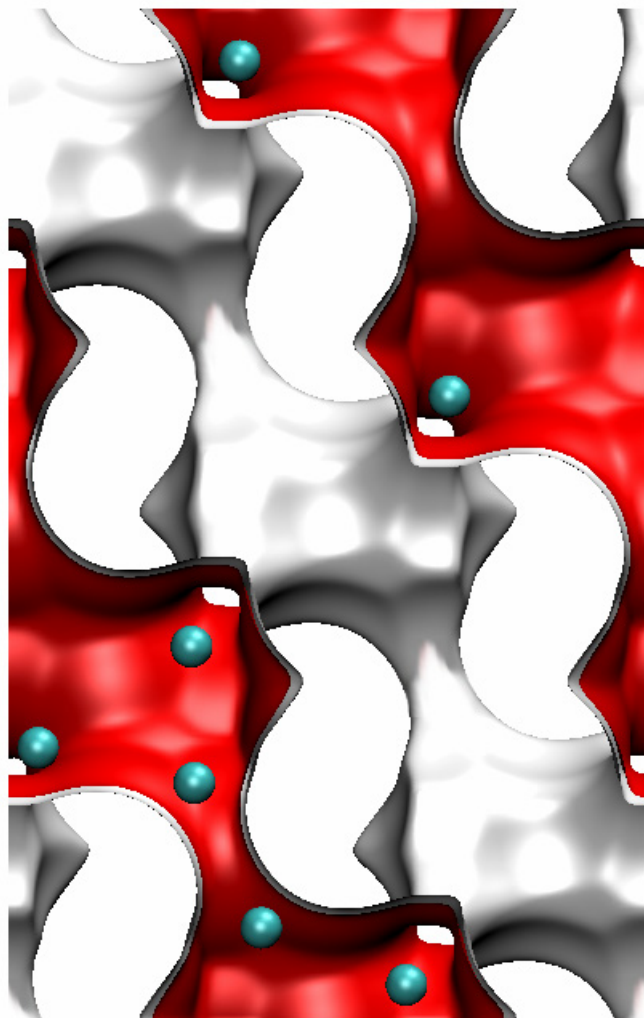
CO$_2$
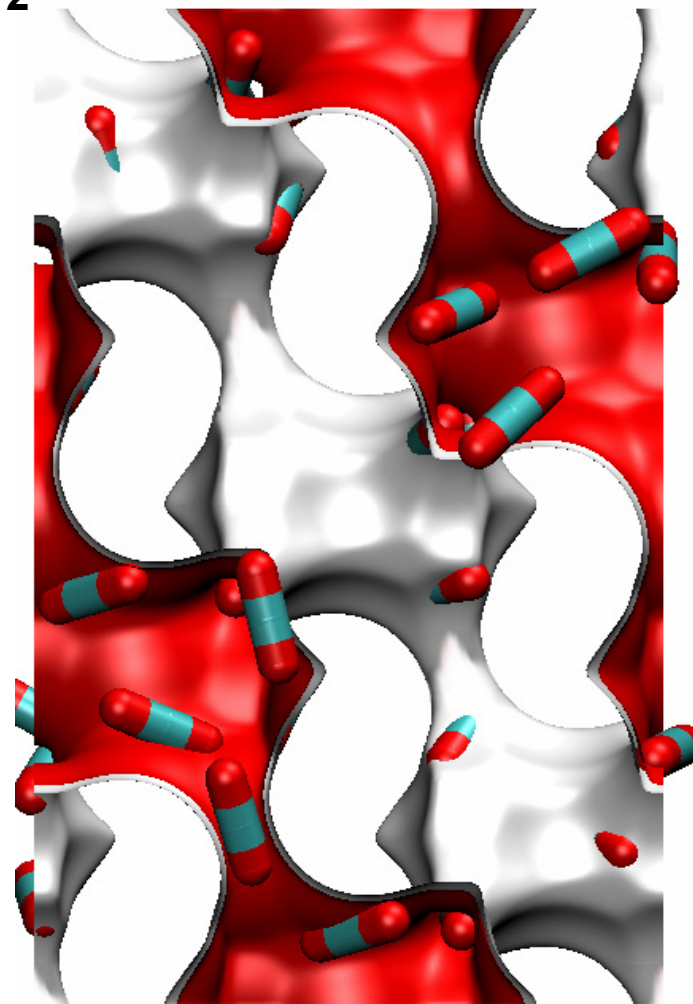
f_i=1000 kPa

CHA, 300 K, pure

N2

$f_i=1000$ kPa

CHA, 300 K, mixture

$$f_{CO2} = 500 \text{ kPa};$$
$$f_{CH4} = 9500 \text{ kPa}$$

ternary

GCMC simulations; $f_1 = f_2 = f_3$

Legend: CH4, CO2, N2

CHA 300 K

Loading, q_i / mol kg^{-1} vs. partial gas phase fugacity, f_i / Pa

binary

Legend: CO2, CH4

GCMC simulations; $f_1 = f_2$

CHA 300 K

Loading, q_i / mol kg^{-1} vs. partial gas phase fugacity, f_i / Pa
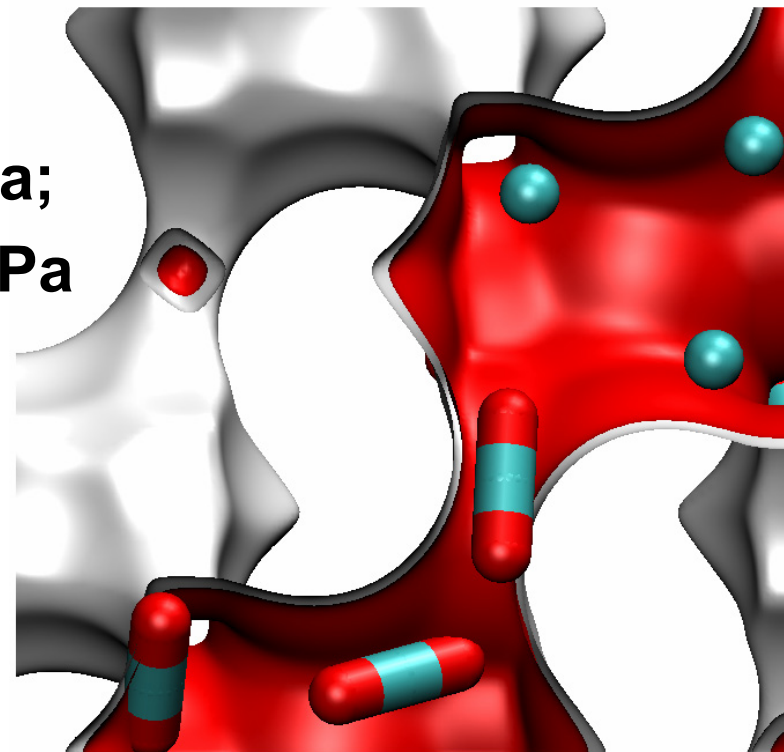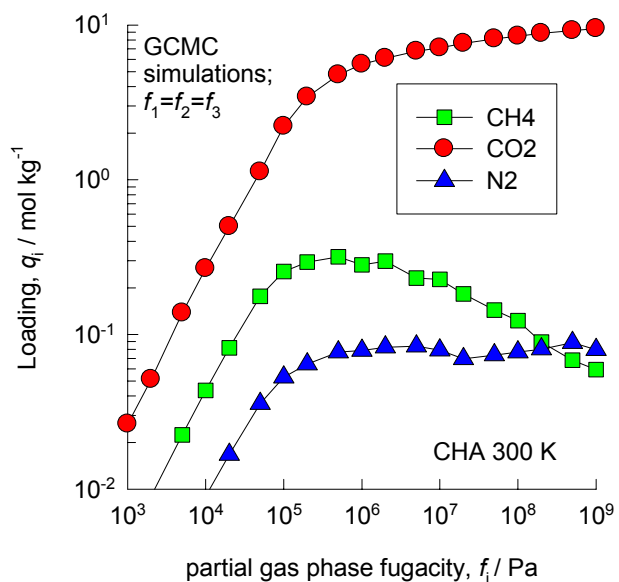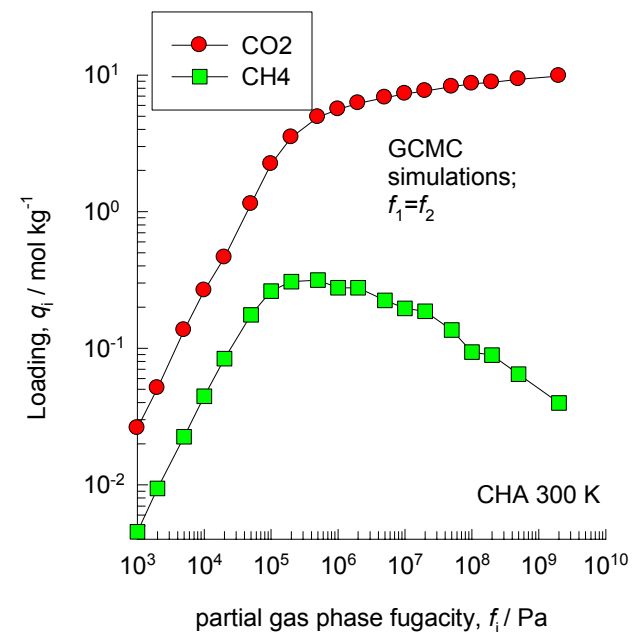
CHA, 300 K, self diffusivities for CO_2 and CH_4
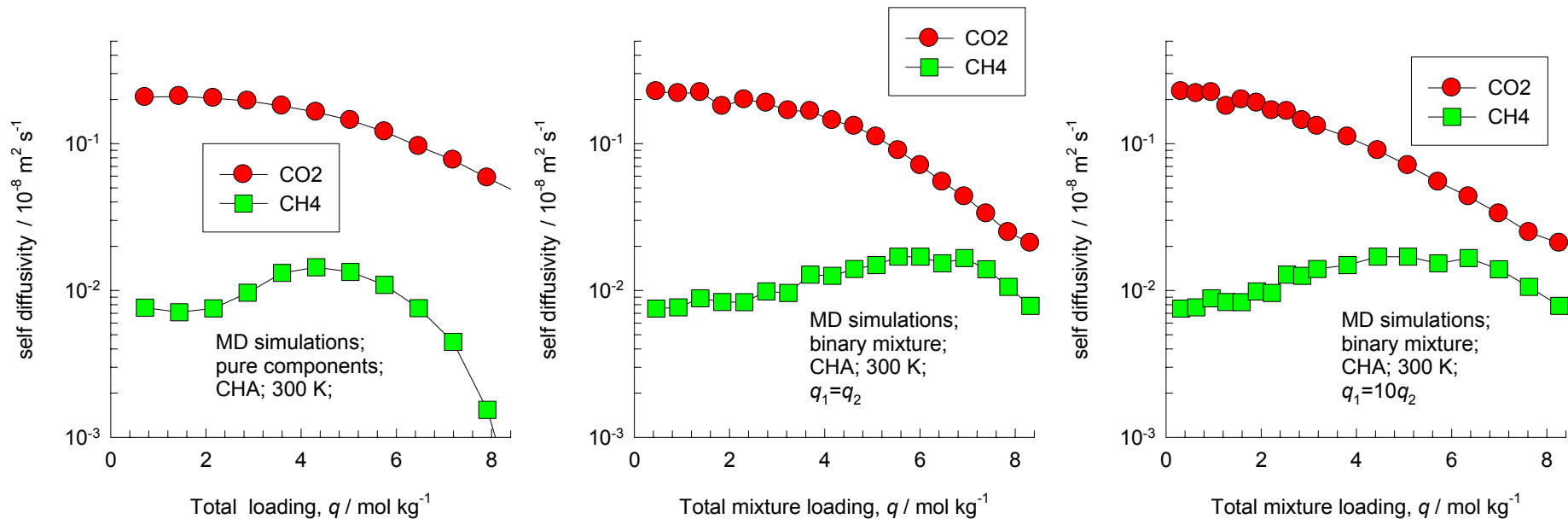
CHA, 300 K, diffusion selectivities
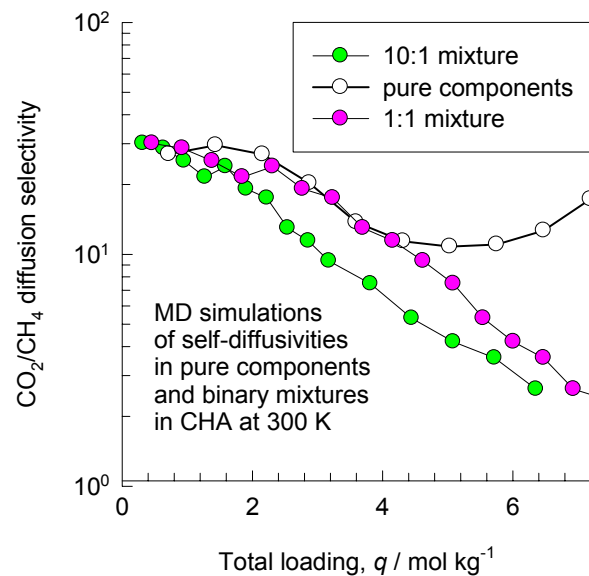
10:1 mixture diffusion data is used in the paper to calculate permeation selectivities

CHA, 300 K, self diffusivities for CO_2 and N_2

self diffusivity / 10^{-8} m^2 s^{-1}

CO2
N2

MD simulations;
pure components;
CHA; 300 K;

Total loading, q / mol kg^{-1}

self diffusivity / 10^{-8} m^2 s^{-1}

CO2
N2

MD simulations;
binary mixture;
CHA; 300 K;
$q_1 = 20q_2$

Total mixture loading, q / mol kg^{-1}

CHA, 300 K, diffusion selectivities

CO_2/N_2 diffusion selectivity

20:1 mixture
pure components

MD simulations
of self-diffusivities
in pure components
and binary mixtures
in CHA at 300 K

Total loading, q / mol kg^{-1}
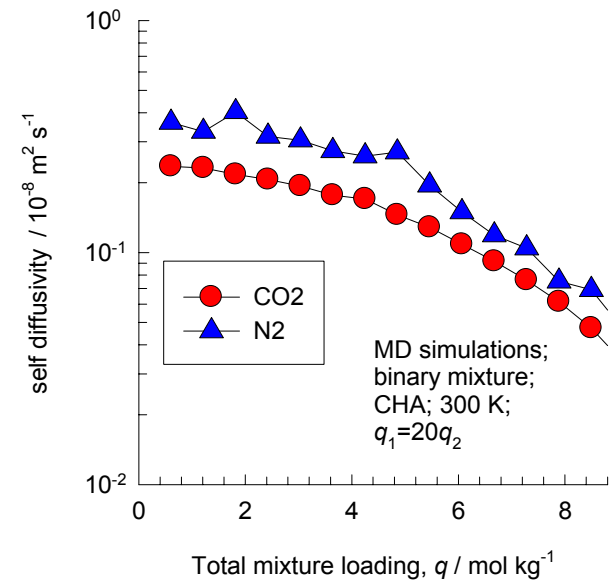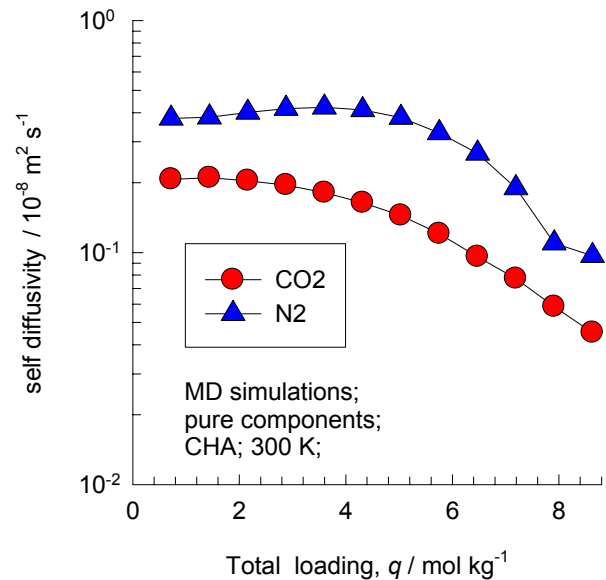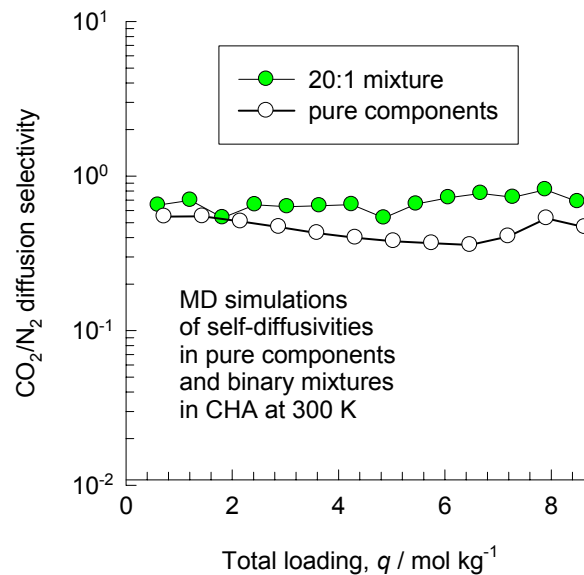
20:1 mixture diffusion
data is used in the
paper to calculate
permeation selectivities

DDR, 300 K, pure
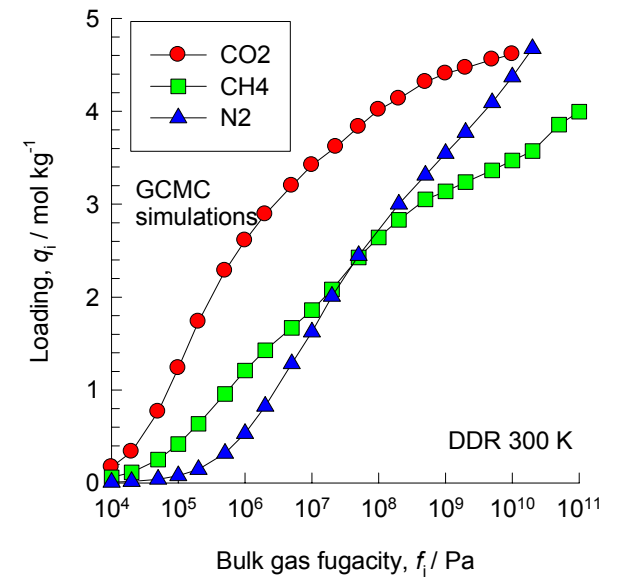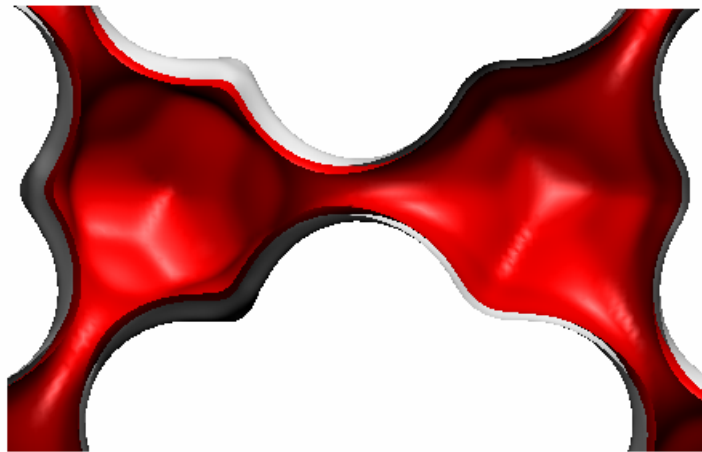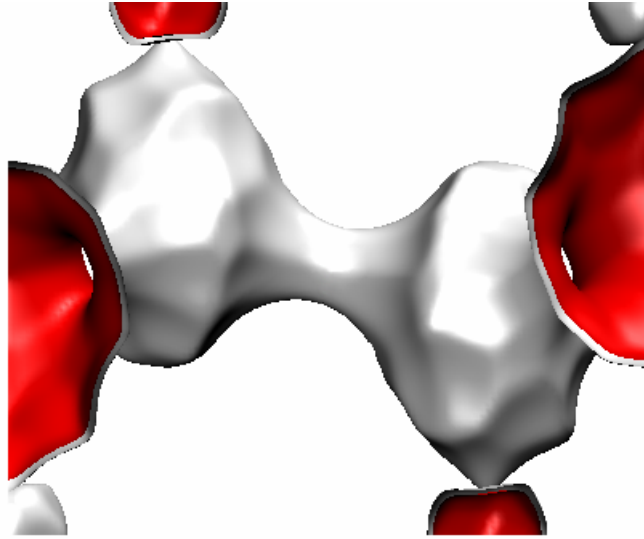
DDR, 300 K, pure CH4
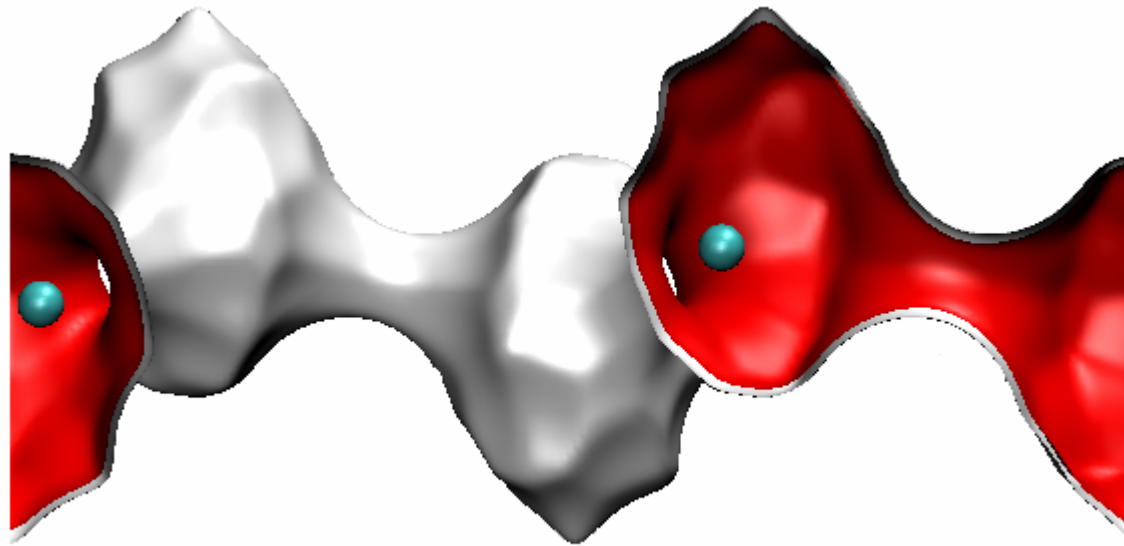
f_i=1000 kPa
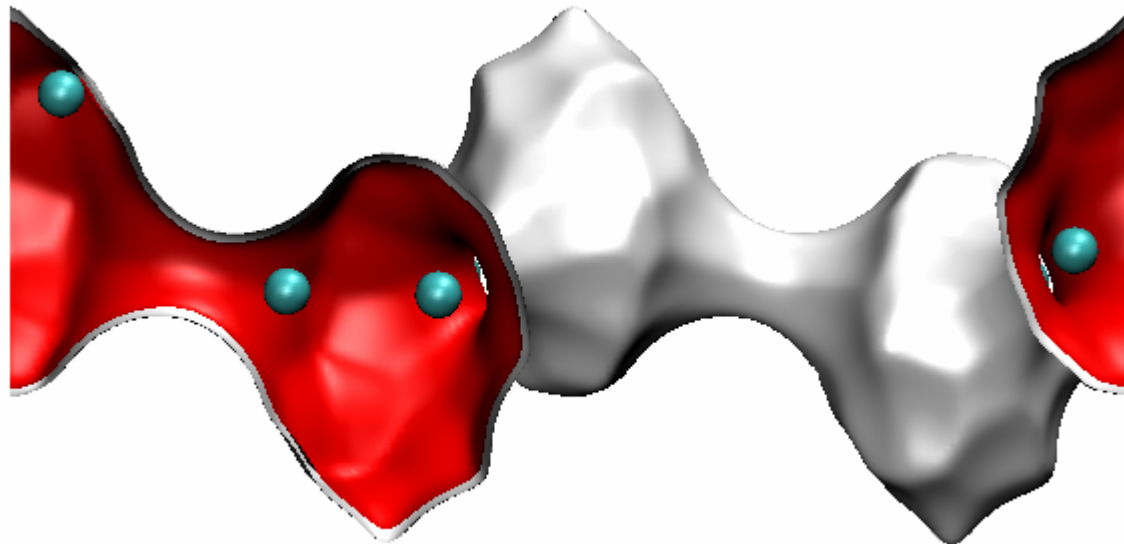
DDR, 300 K, pure CO2
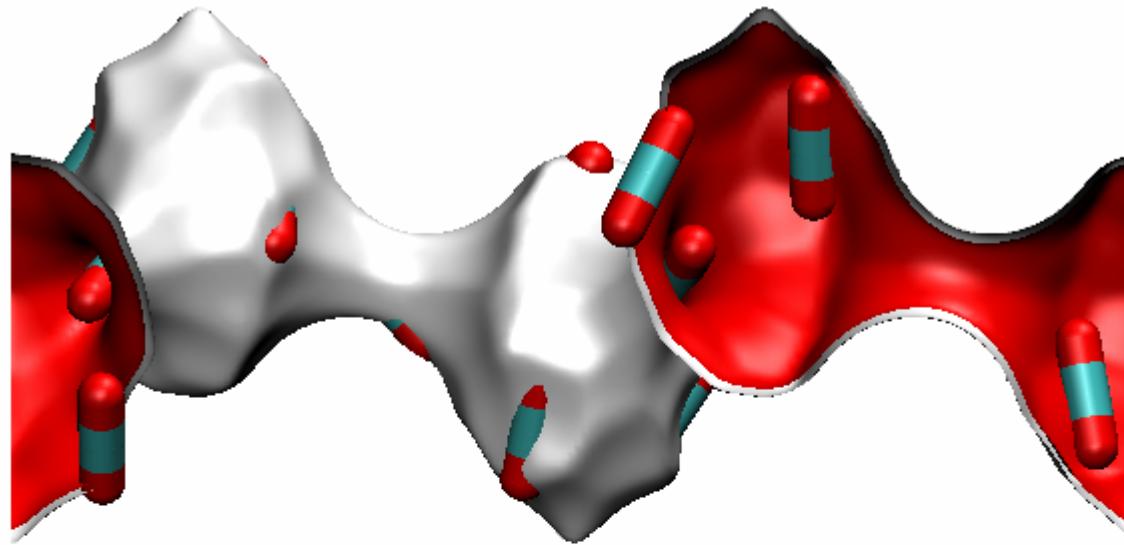
f_i=1000 kPa
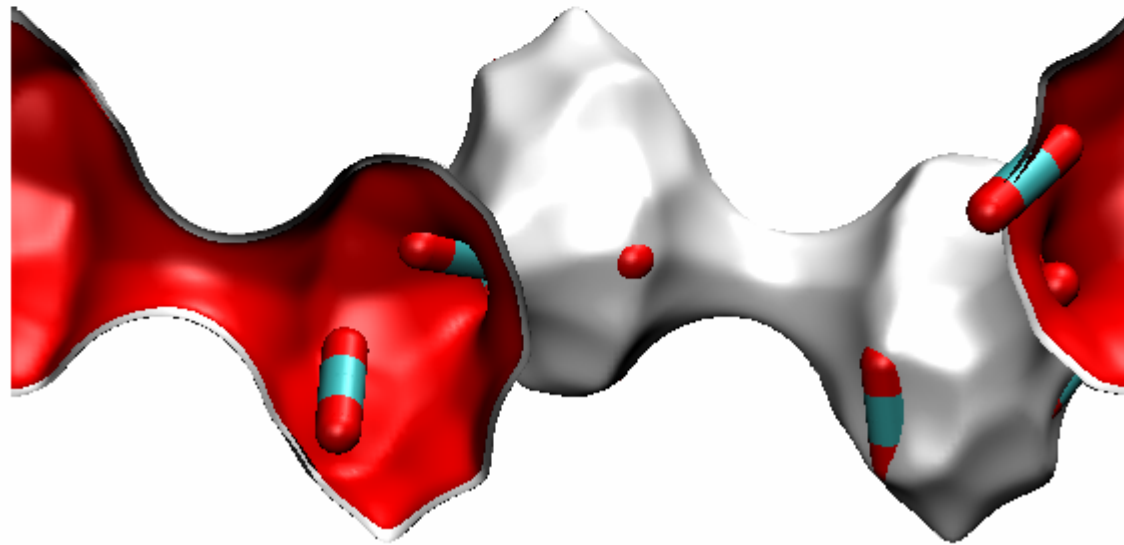
DDR, 300 K, mixture
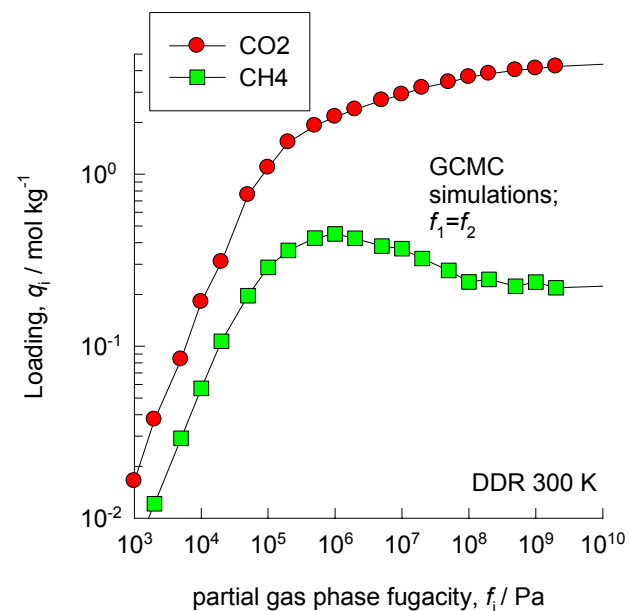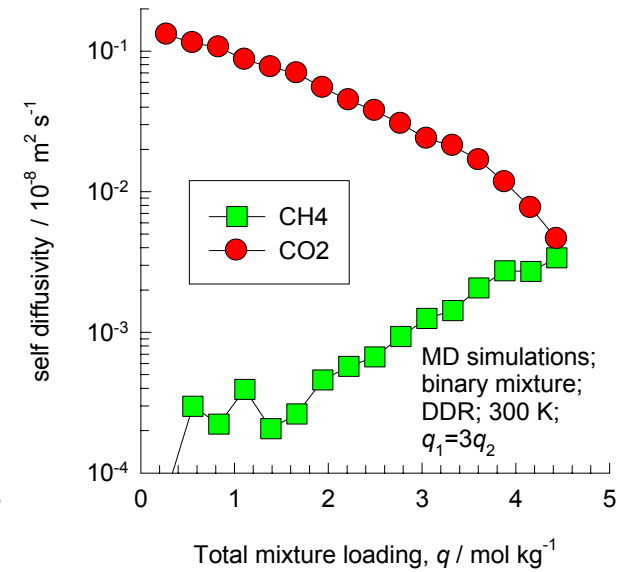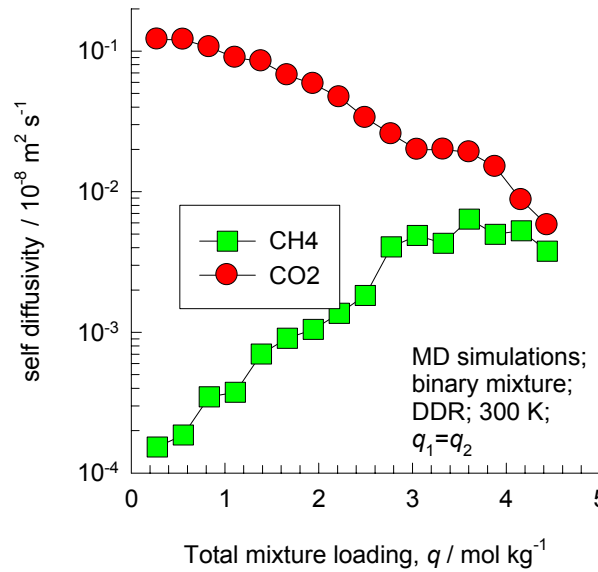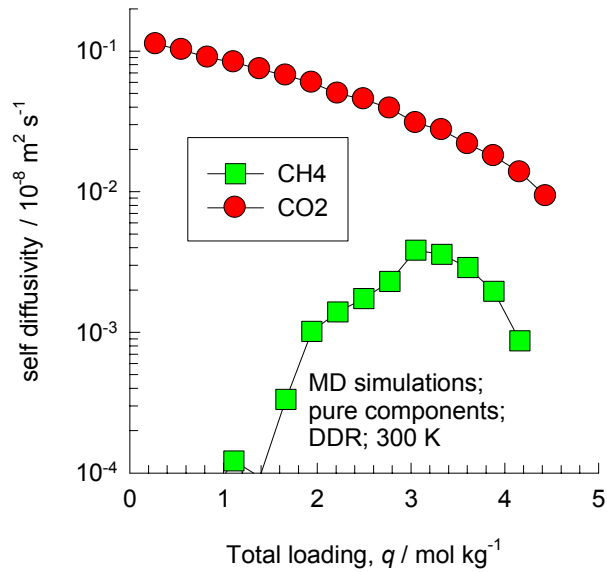
f_{CO2} = 500 kPa;
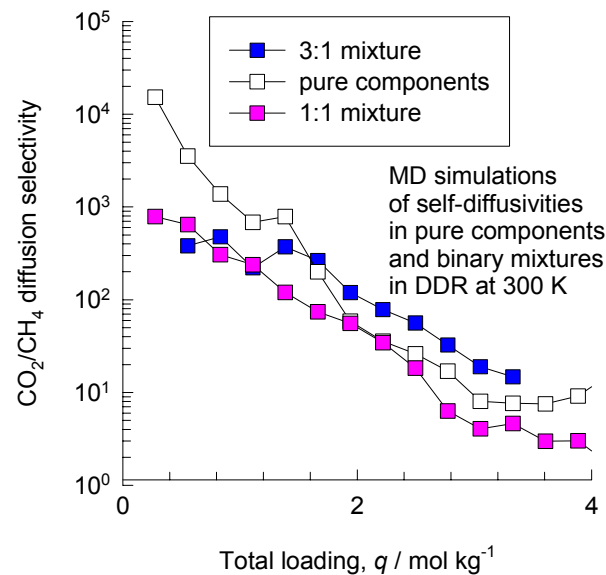f_{CH4} = 9500 kPa
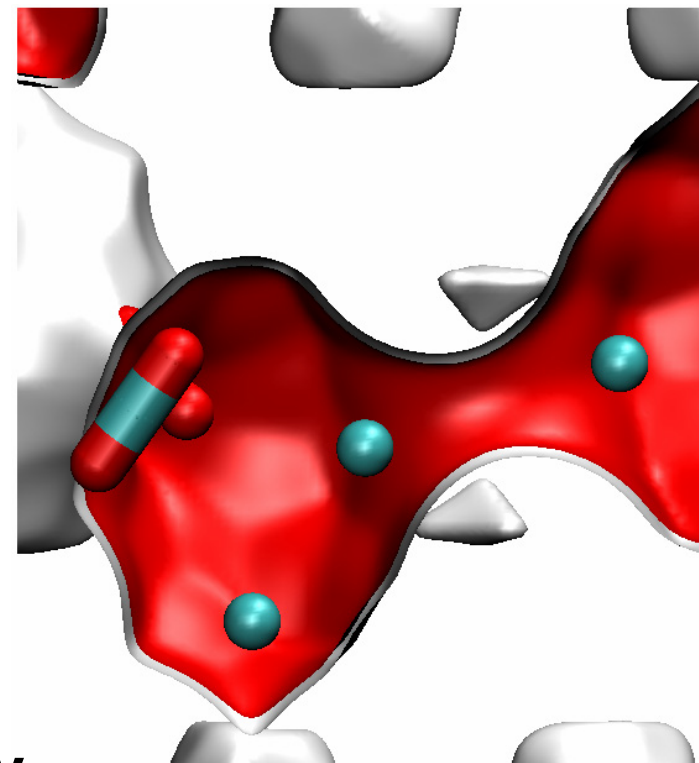
ternary
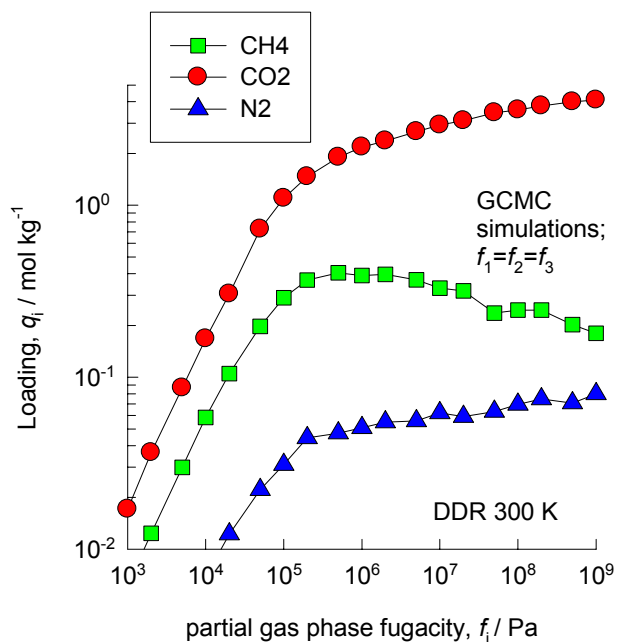
binary

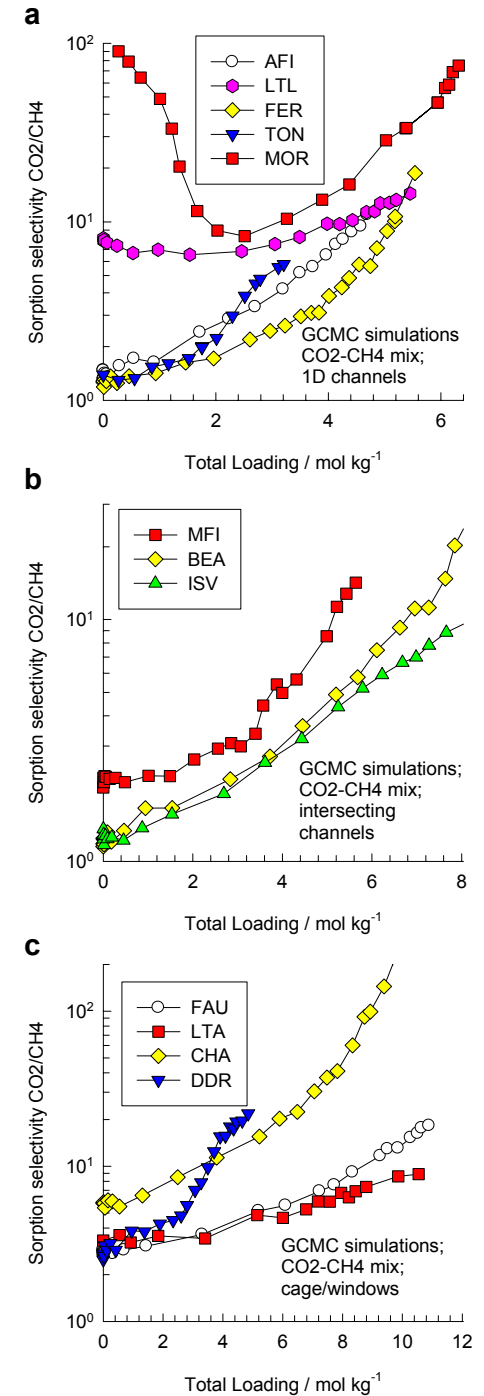# DDR, 300 K, self diffusivities
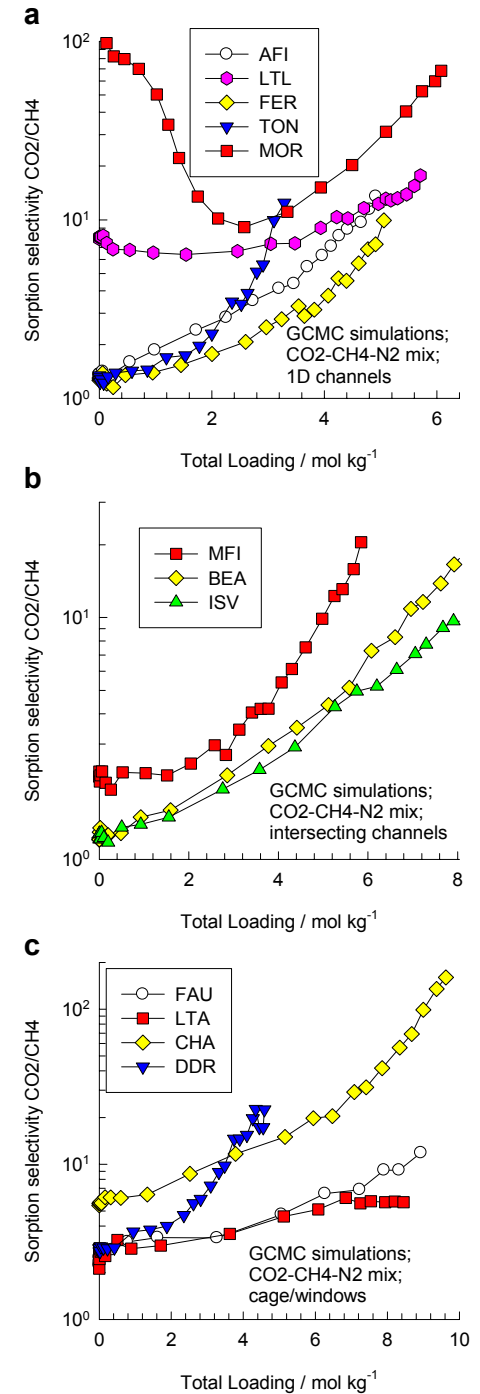

DDR, 300 K, diffusion selectivities

3:1 mixture diffusion data is used in the paper to calculate permeation selectivities
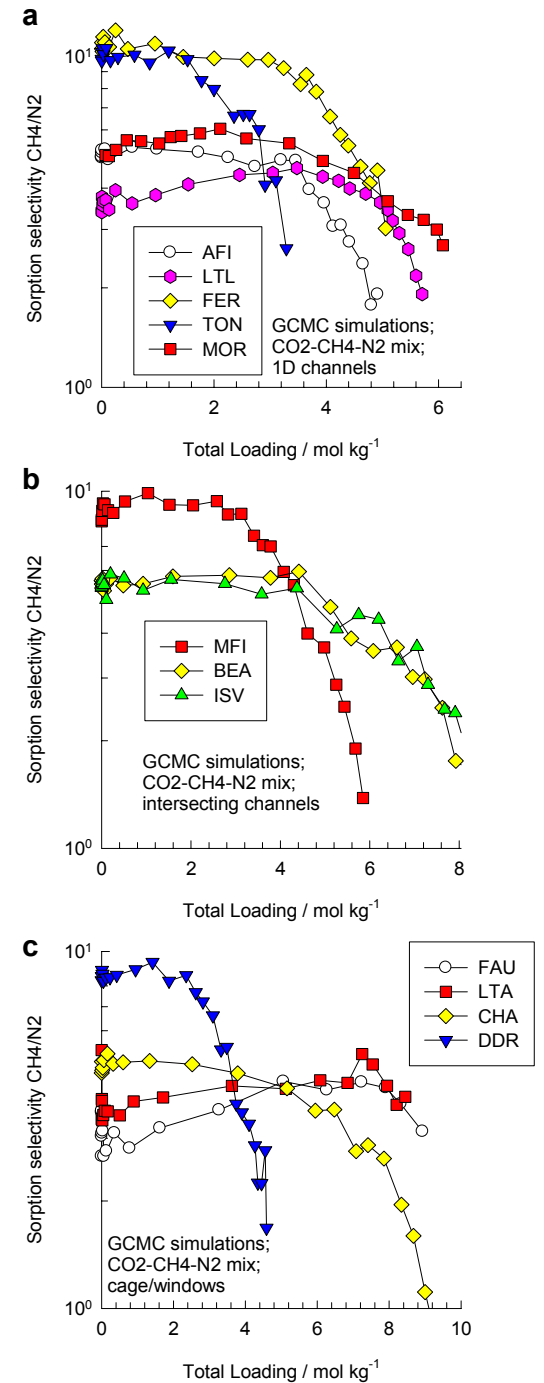
Comparison of CO2/CH4 sorption selectivities based on *binary* mixture data at 300 K in various zeolites

Comparison of CO2/CH4 sorption selectivities based on *ternary* mixture data at 300 K in various zeolites

Comparison of CH4/N2 sorption selectivities based on *ternary* mixture data at 300 K in various zeolites

Comparison of CO2/N2 sorption selectivities based on *ternary* mixture data at 300 K in various zeolites